Chemical Engineering Journal 419 (2021) 129528

Contents lists available at ScienceDirect

Chemical Engineering Journal

journal homepage: www.elsevier.com/locate/cej

From ultrastiff to soft materials: Exploiting dynamic metal–ligand cross-links to access polymer hydrogels combining customized mechanical performance and tailorable functions by controlling hydrogel mechanics

Agniva Dutta [a], Krishanu Ghosal [b], Kishor Sarkar [b], Debabrata Pradhan [a], Rajat K. Das [a,*]

[a] Materials Science Centre, Indian Institute of Technology Kharagpur, Kharagpur 721302, India
[b] Gene Therapy and Tissue Engineering Lab, Department of Polymer Science and Technology, University of Calcutta, 92, A.P.C. Road, Kolkata 700009, India

ARTICLE INFO

Keywords:
Tough
Ultrastiff
Tailorable hydrogels
Resistive Sensor
Capacitive Sensor
Compressible Supercapacitor

ABSTRACT

Recently hydrogels have attracted much attention due to their great potential for a wide range of applications, which require specific set of mechanical properties and customized functions for specific applications. However, traditional hydrogels with inferior mechanical properties lack the scope for wider tuneability. So it becomes a great challenge to prepare a hydrogel system which can cater to wider mechanical and functional needs. This work reports for the first time a facile one step fabrication of Poly(methacrylamide-co-vinylimidazole)-M^{2+} (M = Ni and Zn) fully physically cross-linked hydrogels with fixed total monomer feed concentration and co-monomer ratio, wherein by controlling the kinetics of metal–ligand interactions, the as-prepared hydrogel shows ultra wide spectrum of mechanical properties (Compressive strength ~103 to 247 MPa at 96% strain and compressive stiffness of ~0.434 to 8.944 MPa; elastic modulus ~0.73 to 38.8 MPa; tensile strength ~0.55 to 6.77 MPa; toughness ~1 to 35.88 MJ m^{-3}; strain at break ~332 to 1132%). Furthermore, the presence of pH-responsive metal–ligand cross-links along with hydrophobic methyl group in the backbone allows for pH-dependent tuning of mechanical properties at alkaline pH (Elastic modulus ~155 MPa, tensile strength ~7.2 MPa and compressive stiffness ~36 MPa); The hydrogels demonstrate fast self-recovery, excellent fatigue resistance and efficient self-healing, along with temperature dependent shape memory behaviour. Applications of these hydrogels are demonstrated in highly sensitive flexible resistive (Gauge factor of 11 and 22 at 100 and 200% strain respectively) and capacitive sensors for motion and pressure sensing and as an electrolyte for the fabrication of a compressible supercapacitor (which could withstand ~3000 fold weight of the whole supercapacitor).

1. Introduction

Hydrogels are three-dimensionally cross-linked soft and wet polymeric materials. Because of their stimuli-responsive behaviour and general biocompatibility, potential applications can be envisaged in diverse fields, either as biomimetic materials in tissue engineering [1,2], structural implants [3], drug delivery [4,5], or in sensing and energy storage applications including tactile sensing (strain, pressure and temperature sensor) [6–8], actuators [9,10], soft robotics [10], and as electrolytes in supercapacitors [11,12] and batteries [13,14]. For most of these applications, hydrogels with robust mechanical properties are required. However, because of their high water content and low cross-link density, hydrogels are typically weak and brittle (fracture energy ~10 J m^{-2}). In recent years, several strategies such as double network [15–18], dual cross-linking [19,20], and nanocomposites [21–23] have been successfully applied to improve the hydrogel mechanical properties. Introducing energy dissipating mechanisms into the gel network remains a prominent approach towards this end [24]. For example, Sun et al. synthesized a double network hydrogel by combining alginate and polyacrylamide where the alginate was cross-linked via reversible Ca^{2+}-coordination bond while polyacrylamide was lightly cross-linked through permanent chemical cross linker. When stressed, the polyacrylamide chains held the structure (or bridged the notch) while the coordination bonds unzipped progressively to dissipate applied energy, which eventually led to enormous fracture energy of 9000 J m^{-2} although the stiffness (24 kPa) and tensile strength (160 kPa) remained very low [16]. In another pioneering work, Zhou and coworkers reported a dual cross-linked hydrogel from poly(acrylamide-co-acrylic

* Corresponding author.
E-mail address: rajat@matsc.iitkgp.ac.in (R.K. Das).

https://doi.org/10.1016/j.cej.2021.129528
Received 15 December 2020; Received in revised form 5 March 2021; Accepted 22 March 2021
Available online 27 March 2021

acid), wherein, along with light covalent cross-linking, the acrylic acid group engaged in strong secondary cross-linking (coordination bond) upon soaking into the $FeCl_3$ solution, which effectively dissipated energy leading to a hydrogel which showcased high mechanical strength (~6 MPa) and toughness (~27 MJ m^{-3}) although it remained soft (elastic modulus < 2 MPa) [19].

Most of the hydrogels gain their toughness owing to high stretchability and remain relatively soft (stiffness < 10 MPa), creating impediments for load bearing applications. In comparison with these synthetic hydrogels, for instance, animal cartilage (consisting of ~50% water) is not only significantly stiffer (100 MPa) but is also tough (fracture energy ~1000 J m^{-2}). There are only a few studies in the literature that have reported highly stiff as well as tough hydrogels. Tiller and co-workers have designed ultrastiff hydrogels by employing enzyme-induced mineralization in the gel network [25]. Although these hybrid hydrogels showed high Young's modulus (up to 440 MPa), they displayed very low tensile breaking strain (17%) and a moderate fracture energy (800 J m^{-2}) [25]. In another work, Gong and coworkers have prepared highly stiff (370 MPa) anisotropic hydrogels with aligned fibrous structures. The alignment of polymer chains along the length of the pre-stretched hydrogels was achieved by drying the hydrogels while they were restricted along their length direction. However, the mechanical properties perpendicular to alignment direction were not evaluated. This strategy is also specific for polymers with relatively high rigidity [26]. Apart from these reports, the other approaches towards stiff hydrogels have mainly relied upon dense hydrogen bonded physical cross-links [27–29]. For example, Sheiko and co-workers have developed poly(N, N-dimethylacrylamide-co-methacrylic acid) (P(DMAA-co-MAAc)) based hydrogel and by properly balancing the covalent and hydrogen-bonded cross-linking via controlling the comonomer mixture composition and initiator concentration, displayed high Young's modulus and fracture energy of 28 MPa and 9.3 kJ m^{-2}, respectively with moderate tensile strength of 2 MPa, when incubated in acidic condition (pH = 3) [27]. Liu and coworkers have prepared highly stiff and tough hydrogels (tensile strengths 1.7–4.7 MPa; compressive strengths 6.5–23.4 MPa at 80% compressive strain; elastic modulus 48.4–100.3 MPa and high toughness of 5.66–20.35 MJ m^{-3}) by polymerizing N-acryloylsemicarbazide monomer at different initial concentrations [30]. Because of the simultaneous presence of amide and urea functions on the side chain, the resulting polymer chains formed strong hydrogen bonded cross-links.

The mechanical properties of the stiff hydrogels in these examples have been controlled either by changing the molecular weight of the polymers (changing the initiator concentration), total polymer content (changing the initial monomer concentration), or by controlling the ratio of monomers in the co-polymerization mixture. Thus, the hydrogel mechanics has been controlled by tuning the spatial structure of the network. However, apart from high stiffness, different applications require different customized properties, which are not restricted to the mechanical robustness but require focus on mechanical tunability, stimuli responsiveness, ionic conductivity, self-healing properties, etc. For example, hydrogels mimicking load bearing tissues like cartilage and tendons require simultaneous presentation of high mechanical strength and stiffness, along with high toughness and fracture energy. On the other hand, iontronic applications in flexible devices would require good ionic conductivity and high deformability (stretchability and compressibility) along with good self-recovery property and self-healability. Thus, the ability to access a wide spectrum of mechanical properties in a single hydrogel system is a crucial aspect that requires critical consideration. Clearly, new hydrogel materials with different design strategies need to emerge to expand the utility and applicability of stiff hydrogel materials.

Our previous observation and available literature suggests metal–ligand coordination bond can be highly useful to improve the mechanical properties by effectively dissipating applied energy [16,19,20,31]. To the best of our knowledge, the potential of metal–ligand sacrificial cross-links has not been explored fully to design ultrastiff hydrogels and very few literatures are available. For example, Liang et al. prepared ultrastiff poly(acrylamide-co-acylic acid)/Na-alginate/Fe^{3+} hydrogel through three step process. A key step to get highly stiff hydrogel was immersing in saline water to wash weakly coordinated Fe^{3+} and formation of more crosslinked complexes. Hence mechanical properties were tuned mainly by controlling the co-monomer ratio, where an optimal hydrogel showcased stiffness of 24.6 MPa and toughness of 4800 J m^{-2} [32]. The metal–ligand coordination bond may allow temporal control of hydrogel mechanics independent of, or in combination with spatial structure of the hydrogels [23,33,34]. In a previous report, we have successfully used dynamic Ni^{2+}-imidazole based coordination bonds along with a combination of low density of chemical cross-linking to obtain hydrogels that showcased ultra-fast self-recovery and self-healability [20]. However, these hydrogels exhibited only moderate stiffness (~200 kPa) and tensile strength (<1 MPa). In the present contribution, we report a fully physically cross-linked imidazole based tough and stretchable hydrogel material, which demonstrates an ultra-wide spectrum of mechanical properties along with tailorable functions suited for specific applications. Our design strategy combines metal–ligand cross-links (that should act as sacrificial bonds to dissipate energy and enhance toughness) with acrylamide having methyl substitution (to restrict the chain mobility and thereby increase chain stiffness), allowing us to access hydrogels with ultra-high stiffness, good stretchability, and high fracture energy. We have prepared a physically cross-linked hydrogel from random poly(methacrylamide-co-vinylimidazole) copolymer with fixed total monomer concentration (40 wt%) and co-monomer molar ratio (Methacrylamide: Vinylimidazole = 5:2). The control hydrogel derived from simple one-step synthesis of the copolymer without metal ions resulted in very weak hydrogel which could not be clamped for testing, and was readily soluble in water, which suggests the plausible hydrogen bonding between imidazole and amide group is not sufficient to provide good mechanical strength. In contrast, when the polymerization was carried out in the presence of Ni^{2+} ions, the hydrogel at ligand/metal (L/M) ratio 4 showed fracture energy of 19.95 ± 0.629 kJ m^{-2}, which is not only much higher than the biological load-bearing tissue like cartilage (~1000 J m^{-2}) but also superior to most of the hydrogels reported in literature. Simply by altering the kinetics of metal–ligand cross-links (replacing Ni^{2+} by Zn^{2+} at a fixed L/M ratio or by changing the L/M ratio), we demonstrate that a wide spectrum of mechanical properties can be accessed (from soft hydrogels with elastic modulus ~0.73 MPa to ultrastiff hydrogels with elastic modulus ~40 MPa; from a high of toughness of ~36 MJ m^{-3} to a moderate toughness of ~1 MJ m^{-3}). Because of the presence of pH responsive imidazole-metal ion cross-links and hydrophobic pendent methyl group, exposing to alkaline pH resulted in significant increase in stiffness up to ~155 MPa, allowing further tuning and widening the spectrum of mechanical properties. The hydrogel showed temperature dependent shape memory behaviour, self-healing and robust anti-fatigue characteristics. The ionic conductivity could also be modulated by using different ions. We have also demonstrated application of these hydrogels (1) as strain and pressure sensor with high sensitivity (gauge factor ~22 at 200% strain for resistive strain sensor) and (2) as an electrolyte to fabricate a compressible supercapacitor. Hence we propose a versatile physically cross-linked hydrogel system that can provide platform for multi-dimensional tunability according to our need, with device-level examples. The high ionic conductivity and mechanical responsiveness due to stiff backbone synergistically resulted in a highly sensitive resistive sensor. The high sensitivity obtained for our hydrogels gives it an added advantage over the existing reports to monitor human motion detection [7,35,36]. Apart from these applications, especially the hydrogel containing imidazole-Zn^{2+} interaction (well-known biological interaction) could be explored for biological application due to its dynamic nature and biological resemblance [37]. For instance, bisphosphonate-metal ion dynamic interaction has been used to prepare injectable hydrogels with shear-

thinning and self-healing capabilities. Such hydrogels have been shown to regulate the differentiation of encapsulated stem cells via dual cross-linking strategy [38,39]. Nanocomposite hydrogels based on Mg^{2+}-pamidronate co-ordination have been reported to enhance bone tissue regeneration through a positive feedback loop of alkaline phosphatase expression and drug delivery at the hydrogel injection site [40]. The dynamic nature of the metal–ligand cross-links in our hydrogels with self-healing capability and thixotropic behavior can potentially be used to envisage similar biological applications along with potential targeted drug delivery capabilities utilizing stimuli-responsiveness. The control of hydrogel stiffness from soft to ultrastiff regime can provide a platform to dictate microenvironment dependent cellular response in synthetic scaffolds [41].

2. Experimental

2.1. Materials

Vinyl Imidazole (Sigma-Aldrich, Germany) Methacrylamide (Sigma Aldrich), TMEDA (Loba Chemie), Ammonium Persulfate (APS) (Merck, India) $NiCl_2{\cdot}6H_2O$ (SRL, India) and $ZnSO_4{\cdot}7H_2O$ (Merck, India) were used as received. Deionized water (Millipore, Merck) was used for all the experiments.

2.2. Preparation of hydrogel

The PMAI-M−X gels were prepared in single step. For example, PMAI-Ni-4 was synthesized by dissolving 2.77 g (0.0325 mol) of Methacrylamide, 1.18 mL (0.013 mol) Vinyl Imidazole, and 0.774 g (0.00325 mol) of $NiCl_2{\cdot}6H_2O$ in deionized water (total volume of solution was kept 10 mL) at 30 °C under vigorous stirring (the solution was occasionally vortexed, if needed). After purging with argon gas for 30 min, Ammonium persulfate (1 wt% of total monomer) and TMEDA (20 μL) were added under vigorous stirring and immediately transferred to Petri Dish and kept for 12 h leading to transparent tough hydrogel film. While the PMAI-Zn-4 was synthesized following the above procedure, instead of nickel salt; $ZnSO_4{\cdot}7H_2O$ (0.945 g, 0.00325 mol) was added. The control hydrogel (PMAI) was prepared without addition of any metal salt, utilizing above procedure.

2.3. Characterization

2.3.1. Determination of mechanical properties

All mechanical properties of the hydrogels at room temperature (25 °C) were tested in Zwick/Roell Z050 Universal Testing Machine. A thin coating of silicone oil was given to prevent water removal prior to every test. For tensile test, hydrogel with a thickness of ~1 mm was cut into rectangles (~40 mm in length and ~5 mm in width) by a scissor and grip to grip seperation was kept ~10 mm and the rate of the extension was 100 mm min^{-1} for tensile and cyclic loading–unloading experiments. The compression tests were conducted using cylindrical samples (~ 14 mm diameter and ~16 mm height) at a crosshead speed of 3 mm min^{-1} unless otherwise mentioned.

The engineering stresses (σ) were calculated using the following formula:

$$\sigma = F/A_0 \quad (1)$$

where, F is the applied force and A_0 is the initial Cross-sectional area.

The fracture energy of PMAI-Ni-4 was determined using Rivlin and Thomas's method [42]. To determine the fracture energy, rectangular strips of width 20 mm (a_0), thickness 1 mm (b_0) were prepared and the grip to grip seperation distance was 4 mm. The unnotched sample was stressed to determine the force–length curve while the notched sample with 40% cut (cut through a scissor) gives the critical distance (L_c), a distance at which the crack starts to propagate. The area under the force–length curve upto L_c from unnotched sample gives the work done $U(L_c)$ by the applied force.

The fracture energy of the samples was calculated from the following equation [16]

$$\Gamma = U(L_c)/a_0 b_0 \quad (2)$$

where, a_0 and b_0 are width and thickness respectively.

2.3.2. Determination of water content of the hydrogels

The water content of the hydrogel was calculated by using the following formula:

Water content = $(w_n\text{-}w_d)/w_n$, in which w_n and w_d are the masses of the hydrogel in the native and dried states, respectively.

2.3.3. Fourier transform infrared spectroscopy (FTIR)

The FTIR spectra of dried hydrogel films were recorded using Perkin Elmer spectrum-II spectrometer.

2.3.4. Thermogravimetric analysis (TGA)

The thermograms of the native and thin silicone oil coated hydrogel films were recorded at a heating rate of 5 °C min^{-1} from 30 to 90 °C using TA instrument (TGA Q50).

2.3.5. Dynamic mechanical analysis (DMA)

The NETZSCH DMA-242 E Artemis instrument (Netzsch, Germany) was used to evaluate the storage and loss moduli of cylindrical (~10 mm diameter and ~5 mm height) hydrogel (coated with silicone oil) samples in compression mode at 1 Hz as a function of temperature (ranges from 30 °C to 90 °C) under nitrogen atmosphere with a heating rate of 5 °C min^{-1}, and load was set at 4 N.

2.3.6. Rheology

The rheological properties of PMAI-Ni-4, PMAI-Zn-4 and PMAI-Zn-4 swelled in different pH was evaluated using Anton paar parallel plate rheometer MCR 102 with plate diameter of 25 mm at 25 °C and the gap was kept nearly 1–1.1 mm. The strain sweep experiments were measured at constant frequency of 1 Hz and frequency sweep were measure from 0.1 to 100 Hz at 0.1% strain. The intrinsic self-healing property (thixotropy) was examined by subjecting the gel with alternative strain before (linear region) and after cross-over point respectively for 3 min each at constant frequency of 1 Hz.

2.3.7. Self-healing property

The self-healing property of the hydrogel sample was examined by cutting the hydrogel sample into two halves and then the same was joined together, heated at 37 °C for predetermined time inside a sealed plastic bag with silicone oil coating, to prevent water removal.

2.3.8. Shape memory behaviour

A straight rectangular stip of PMAI-Ni-4 twisted into a helix and put into a plastic tube and kept at 10 °C for 30 min to fixed the temporary shape. The shape memory bahaviour was studied by immersing the sample under silicon oil at 50 °C.

2.3.9. Ionic conductivity measurements

The PMAI-M−X rectangular strip (Width 5 mm, length 10 mm and thickness 1 mm) was used to measure the ionic conductivity. The Electrochemical impedance spectra was measured by Gamry Reference 3000 galynostat from 100 Hz to 1 MHz frequency at room temperature using a platinum four probe conductivity cell (Electrochem Inc., FC-BT-115). The ionic conductivity (σ, S/cm) was measured using the following equation.

$$\sigma = \frac{L}{R \times A} \quad (3)$$

where R, resistance calculated from Nyquist plot. L is the distance between electrodes (0.425 cm) and A is the effective area (Width × Thickness).

2.3.10. Tactile sensing

Resistive and capacitive sensors were prepared from the PMAI-Zn-X conductive gels using conductive copper tape (to make connection) and commercially available adhesive dielectric tape (VHB 4910, 3 M). The resistive sensors were prepared by sandwiching the conductive gel in between two VHB tapes (to prevent the water evaporation), while for the capacitive sensor, the dielectric (VHB) was sandwiched between two conductive gel followed by a layer of VHB tape to prevent water removal. The I(Current) vs V(Voltage) and I(Current) vs t(Time) was measured in Keithley 4200 SCS machine for resistive sensors. The capacitance, C and C vs t at a fixed frequency of 10 kHz was measured using Hioki LCR meter for capacitive sensors.

2.3.11. Electrochemical measurements

The supercapacitor devices were prepared by sandwiching the ion conducting hydrogel between two activated carbon coated graphite sheets. Electrochemical performance of such two-electrode supercapacitor devices were charecterized by cyclic voltametry (CV), galvanostatic charge–discharge (GCD) and electrochemical impedance spectroscopy (EIS) measurements using CHI 760D electrochemical workstation (CH Instruments, Inc., USA). The specific capacitance of the fabricated devices was measured from the GCD profile utilizing the following equation [11].

$$C_s = \frac{4 \times I \times \Delta t}{m \times \Delta V} \quad (4)$$

where, I is the discharge current, Δt is the discharge time and ΔV is the potential window during the discharge and m is the mass of active material.

3. Results and discussion

3.1. The effect of L/M ratio on hydrogel mechanical properties

3.1.1. Tensile experiments

The Poly(methacrylamide-co-vinylimidazole) random copolymer, which is denoted as PMAI was synthesized using Ammonium persulfate (APS) and N,N,N′,N′-tetramethylethylenediamine (TMEDA) free radical redox initiator accelerator system without using any chemical cross-linker in deionized water (Scheme 1). The copolymerization of methacrylamide (MA) and vinylimidazole (VIMZ) with molar ratio of 5:2 (MA:VIMZ) and 40 wt% total monomer concentration led to a very weak hydrogel, which was not suitable for mechanical testing. The weak mechanical property shows that, in the absence of any chemical cross-linker, the hydrogen bonding physical cross-links between imidazole and amide group was not sufficient to form a robust hydrogel. The chemical structure of the dried PMAI polymer hydrogel was characterized by FTIR spectroscopy. Fig. S1 shows the major band from the imidazole at 1484 cm^{-1} (C═C and C═N stretching), 1385 cm^{-1} (ring stretching), 1230 cm^{-1} (CH in-plane bending and C-N ring stretching), 1083 cm^{-1} (CH in-plane bending and ring stretching) and 921 cm^{-1} (ring stretching and in-plane bending), while the band at 1650 cm^{-1} corresponds to C═O (amide I) and the shoulder associated with it at 1595 cm^{-1} is due to CN resonance, characteristic to polymethacrylamide [43,44].

Next, the metal–ligand reversible cross-links were introduced by carrying out the co-polymerization in the presence of Ni^{2+} ions (these hydrogels are henceforth denoted as PMAI-M−X, where M and X refer to the metal ion and VIMZ/metal ion ratio (L/M), respectively). The formation of imidazole-Ni^{2+} co-ordination bond was studied by UV–vis (Fig. S2, Supporting Information) and FTIR spectroscopy (Fig. S1A,B). When the UV–vis spectra of dried PMAI (without metal ion) and representative PMAI-Ni-4 gel films were compared, the later showed absorption at 372 and 609 nm while the PMAI absorption spectrum remained nearly flat. The presence of characteristic absorption peak in PMAI-Ni-4 metallogel indicates the formation of imidazole-Ni^{2+} coordination [20,45]. Further confirmation for the presence of metal–ligand interaction is obtained by comparing the FTIR spectra of dried PMAI (control) and PMAI-Ni-4 gels (Fig. S1). The absorptions at 1484 cm^{-1} (C = C and C = N stretching) and 1083 cm^{-1} (CH in-plane bending and ring stretching) in control are shifted to 1486 cm^{-1} and 1093 cm^{-1}, respectively in PMAI-Ni-4 and new band forms at 942 cm^{-1}. These results collectively suggest the formation of Ni^{2+}-imidazole complex in the hydrogels [43,46]. Tensile experiments indicated that the mechanical properties of the resultant metallogels could be tuned significantly by altering the ligand/metal (L/M) molar ratio. By varying the VIMZ/Ni^{2+} ratio, the elastic modulus could be varied from 2.85 ± 0.046 MPa to 38.79 ± 0.87 MPa, strain at break from 693.16 ± 59% to 1184.03 ± 70.37%, tensile strength from 1.98 ± 0.07 MPa to 6.77 ± 0.39 MPa and toughness from 11.47 ± 0.64 MJ m^{-3} to 35.88 ± 1.29 MJ m^{-3} (Fig. 1 A-F). The yielding observed for these hydrogels and the nature of the stress–strain response are representative for tough rubbery hydrogels, as has been reported previously [16,19,47]. The presence of yield suggests the rupture of sacrificial imidazole-metal ion cross-links [48]. The

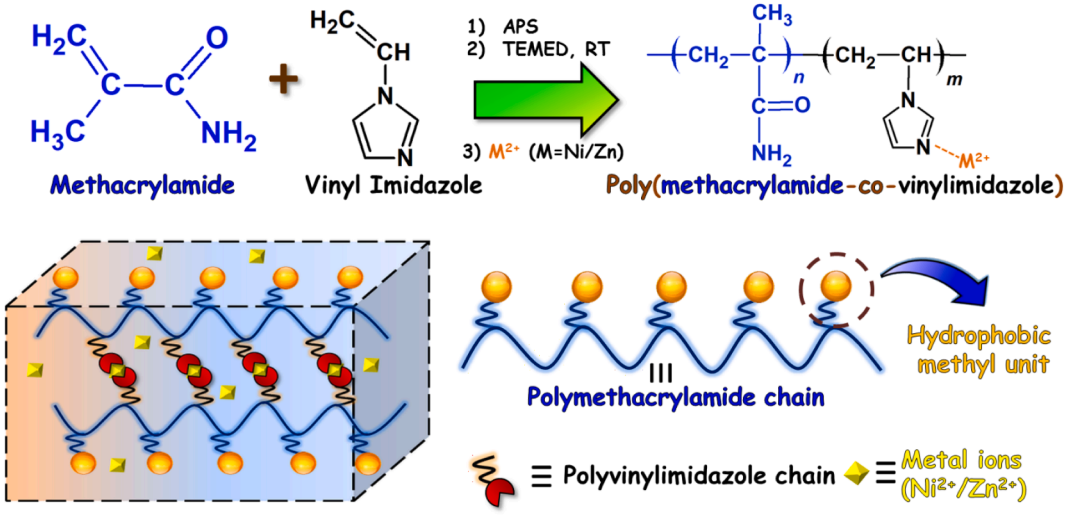

Scheme 1. Synthesis of PMAI-M−X (M stands for metal ions and X stands for vinyl imidazole (ligand) and metal ion ratio respectively).

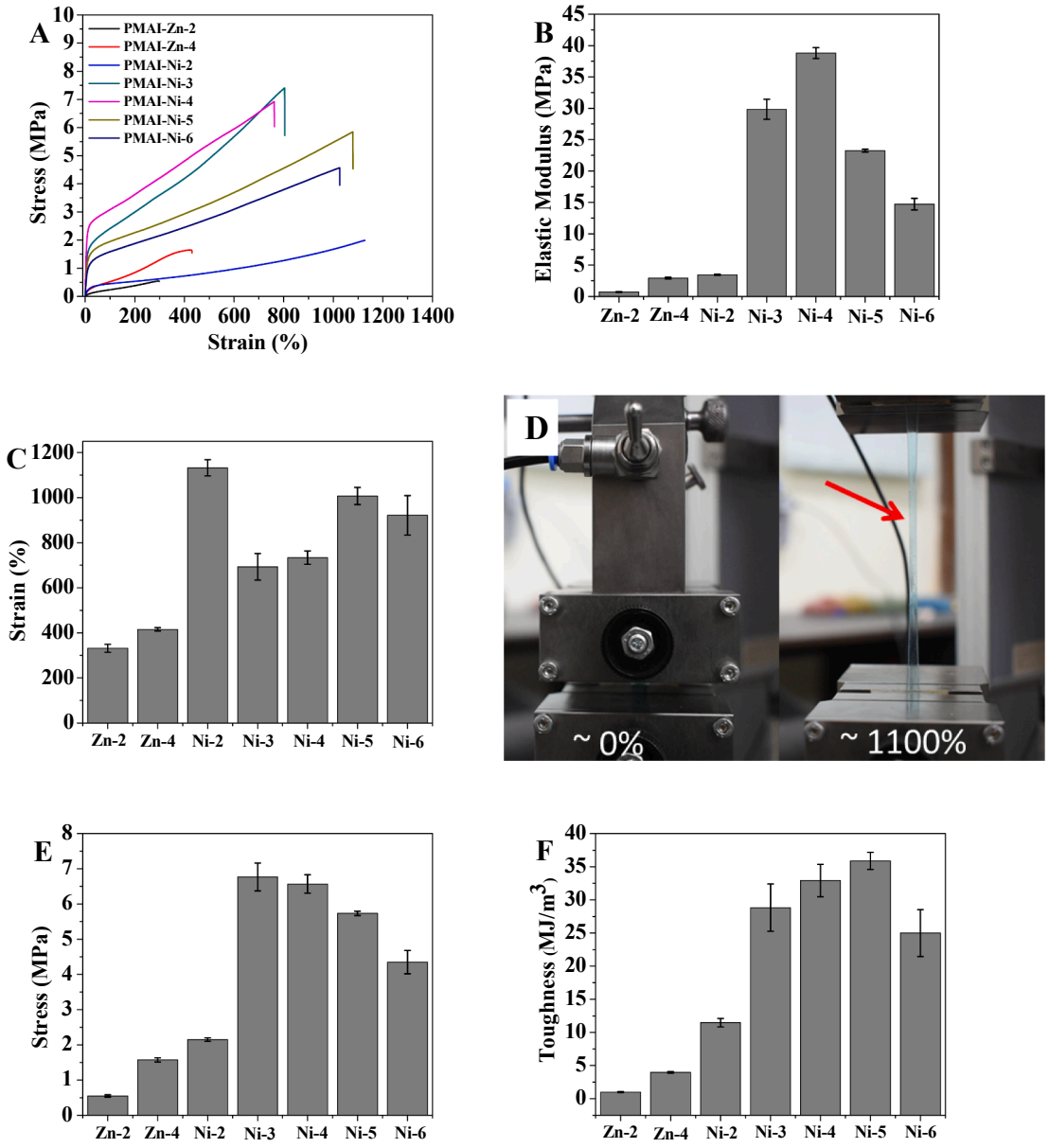

Fig. 1. A) Tensile Stress–strain curve, B) elastic modulus and C) strain at break of PMAI-Zn-2, 4 and PMAI-Ni-X hydrogels. D) Photographs of tensile testing of PMAI-Ni-2 at~ 0 and~ 1100% strain. E) Tensile strength, F) toughness of PMAI-Zn-2, 4 and PMAI-Ni-X hydrogels. Error bars indicate standard errors of mean (n = 3).

tensile strength as well as elastic modulus (stiffness) increase to a maximum at ~L/M ratio of 4. Both low, as well as high concentration of metal ion has a detrimental effect on the mechanical properties. These results establish that metal–ligand cross-links dictate mechanical properties in this class of hydrogel materials. Controlling the kinetics of metal–ligand cross-links can introduce temporal hierarchy in hydrogel mechanical properties [33,49]. In the present work, the Ni^{2+}-imidazole cross-link kinetics is controlled by changing the L/M ratio. The metal ion can interact with up to four imidazole units [50]. As the L/M ratio increases progressively beyond 4, free imidazole ligands are available which increase the rate of ligand exchange [34], facilitating the network relaxation, and hence reducing the network rigidity. Thus, the tensile strength as well as the stiffness of the hydrogel decrease progressively as the L/M ratio is increased beyond 4. Around L/M ~4, almost all the imidazole ligands are engaged in co-ordination with the Ni^{2+} ions, and hence the non-availability of free ligands reduces the rate of ligand exchange significantly, thereby increasing the rigidity of the material. Hence, the strength and stiffness of the hydrogel reach the maximum around L/M ~4. As the metal concentration is increased further, thereby decreasing the L/M ratio (which goes below 4), complexation may happen with simultaneously low and high co-ordination number [51]. Hence, the average number of imidazole ligands involved at a cross-linking site decreases, leading to deterioration of mechanical properties. Apart from the L/M ratio, the metal–ligand exchange kinetics also depends on the nature of the metal ion involved in the cross-links. It has been reported that histidine-Ni^{2+} cross-links relax much slower compared to histidine-Zn^{2+} cross-links, indicating significantly faster ligand exchange kinetics in Zn^{2+} complexes [33]. The imidazole-metal ion complex can be considered to be a close mimic of histidine-metal complexes. Thus, we envisaged that the more labile imidazole-Zn^{2+} cross-links may allow further tuning of hydrogel mechanics. Faster network relaxation in the case of Zn^{2+} based metallogel should lead to significantly softer hydrogel network [34]. For metal–ligand cross-linked networks, dynamic viscosity has been found to be inversely related to the ligand-exchange kinetics [52,53]. Hence, slower rate of ligand-exchange is expected to be associated with increased rigidity of

the network in response to the applied load. Indeed, a drastic reduction in mechanical properties was observed when the hydrogel formation was realized with Zn^{2+} ions instead of Ni^{2+}. For instance, for L/M ratio of 4, the elastic modulus of the hydrogel reduced from 38.79 ± 0.87 MPa for Ni^{2+} metallogel to 2.935 ± 0.13 MPa for Zn^{2+} metallogel, strain at break from 733.96 ± 29.54% to 415.73 ± 7.38%, tensile strength from 6.57 ± 0.26 MPa to 1.57 ± 0.058 MPa and toughness from 32.91 ± 2.44 MJ m^{-3} to 3.96 ± 0.12 MJ m^{-3}. The hydrogels have moderate water content of 45–52 wt% (Table S1). The variation of water content in this range does not influence the mechanical properties of these materials, which are governed by L/M ratio and ligand exchange kinetics of the cross-links. For instance, the PMAI-Ni-4 and PMAI-Zn-4 hydrogels have similar water content (~52 wt%), but the latter is significantly softer due to the more labile imidazole-Zn^{2+} cross-links. These results demonstrate temporal control over hydrogel mechanical performance independent of spatial structure of the hydrogels. Such orthogonal control has previously been demonstrated with kinetically distinct metal–ligand cross-links incorporated into hydrogels [33]. However, to the best of our knowledge, our results demonstrate for the first time that simply by altering the kinetics of ligand exchange for the dynamic metal–ligand cross-links (either by altering the L/M ratio, or by changing the metal ion), in combination with the presence of a chain stiffening

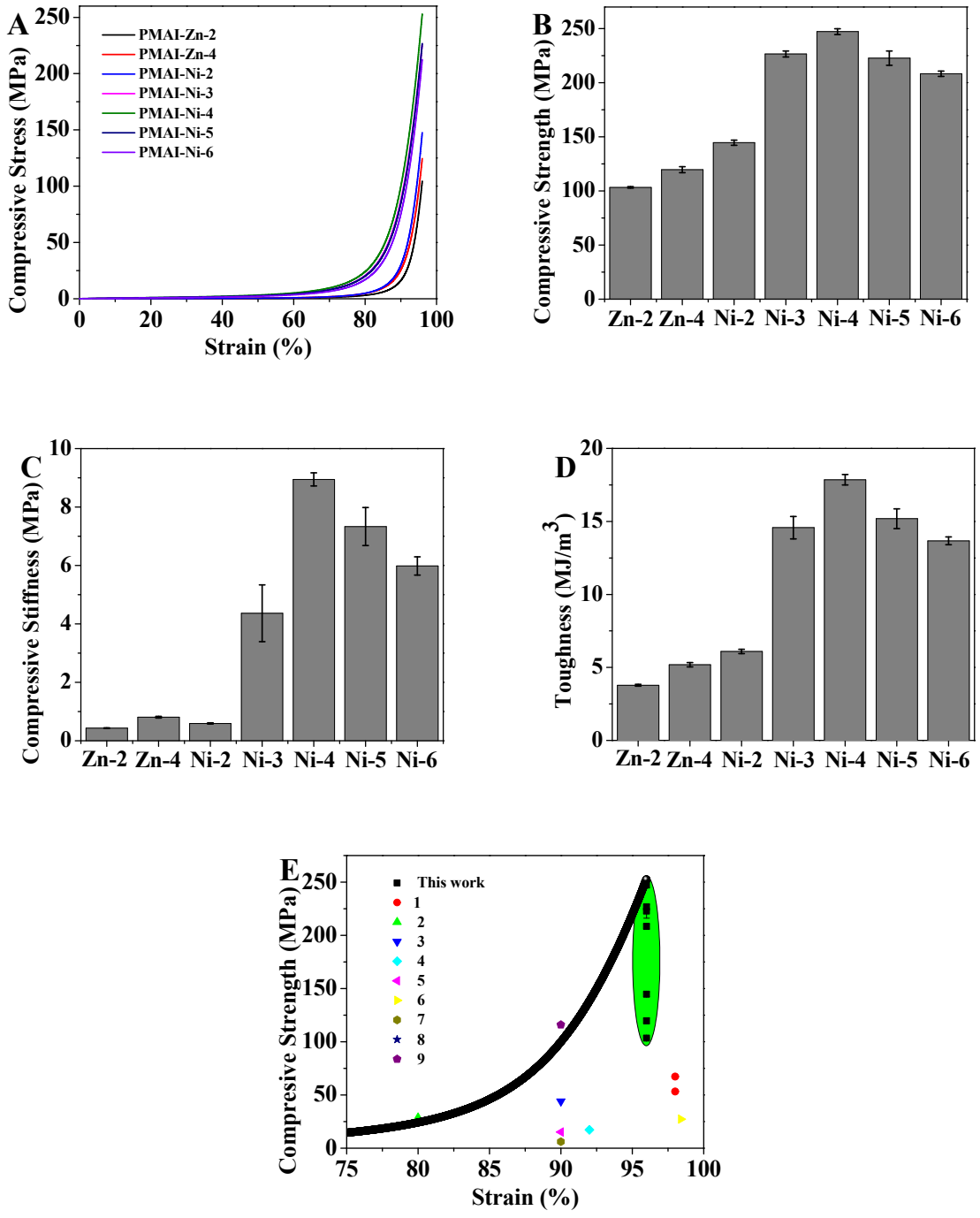

Fig. 2. Compressive A) stress–strain curve B) strength C) stiffness and D) toughness of PMAI-Zn-2,4 and PMAI-Ni-X hydrogels and E) comparison with the state of art (1–8), the green circle shows the range of PMAI-M−X hydrogel series, black line shows PMAI-Ni-4 representative strength vs stain curve and 1 (metal–ligand) [51], 2 (dual physical cross-linking) [31], 3 (metal–ligand) [32], 4 (DN hydrogel) [15], 5 (mineralized hydrogel) [65], 6 (dynamic covalent bond) [66], 7 (nanocomposite) [22] and 8 (anisotropic multilayer hydrogel) [67].

methyl group –whilst the molar ratio of the monomers is kept constant- a wide spectrum of mechanical properties can be accessed, resulting in both soft (elastic modulus ~0.73 MPa) as well as ultra-stiff (elastic modulus ~40 MPa) [27] hydrogels, showing the importance of different hierarchical mechanics present in these physically cross-linked hydrogels. It is important to note that the decrease in VIMZ/Zn^{2+} ratio (PMAI-Zn-2) imparts similar effect (Fig. 1A-C and E-F) as observerd in PMAI-Ni series. Moreover, the PMAI-Ni-4 hydrogel showed significantly high fracture energy of 19.95 ± 0.63 kJ m^{-2} in the pure shear test (Fig. S3, Supporting Information), which is ~20 times higher than that of cartilage (~1000 J m^{-2}), indicating the potential of these hydrogel materials in load-bearing applications.

3.1.2. Compression experiments

After observing the striking effect on mechanical properties in terms of external tensile forces, we investigated the hydrogel performance when subjected to compression experiments. Compressive property (strength) was also found to be highly dependent on the ratio of VIMZ/Ni^{2+} as well as on the choice of the metal ion (Ni^{2+} vs Zn^{2+}), thus providing a great platform for multi-scale tuneability, over a broad range of compressive strengths. The compressive strength varied from 144 MPa for PMAI-NI-2 to 247 MPa for PMAI-Ni-4 at 96% strain (video S1, Supporting Information), compressive modulus changed from 0.593 ± 0.0171 to 8.944 ± 0.225 MPa and compressive toughness varied from 6.09 ± 0.15 to 17.85 MJ m^{-3} (Fig. 2A-D). Initially, with increase in VIMZ/Ni^{2+} ratio, the compressive strength and stiffness increased and reached the maximum at ratio equals 4 and then started to decrease. The corresponding Zn^{2+} based metallogel (PMAI-Zn-4) showed a compressive strength of 119.7 MPa, compressive modulus of 0.805 ± 0.0285 MPa and compressive toughness of 5.19 ± 0.148 at 96% strain. These values are significantly lower than those of its Ni^{2+} counterpart (Fig. 2A, B and C). Further decrease in VIMZ/Zn^{2+} (PMAI-Zn-2) led to decrease in the mechanical properties (Compressive strength 103 MPa, compressive modulus 0.434 ± 0.0104, and compressive toughness 3.78 ± 0.064). These results are consistent with the data from the tensile experiments (vide supra). It is worth to mention that none of the hydrogels fractured even after sustaining this high amount of compressive load. These hydrogels not only show higher compressive strengths than most of the state-of-the-art hydrogel materials reported in the literature, but also for the first time allow us to avail a vast range of strengths by simply tuning the temporal reversible interaction (Fig. 2E). Since the compressive strength has strong dependence on the compressive strain, this comparison is relevant at comparable strains. Hence, a representative compressive stress–strain data for the PMAI-Ni-4 hydrogel is added in Fig. 2E, which shows that the reported class of hydrogels in this work indeed possess high compressive strength compared to the literature. Taken together, these results suggest that by controlling the temporal hierarchy, we can access hydrogels with tailor-made mechanical properties that can be tuned according to the requirement of the specific application.

3.2. The effect of pH on hydrogel mechanical properties

The presence of imidazole-metal ion dynamic bonds imparts pH responsive properties to the hydrogel. The imidazole nitrogen gets protonated at acidic pH, thereby destabilizing the imidazole-metal ions co-ordination bond, whereas the bond remains stable in the basic medium. PMAI-Ni-4, with the better mechanical strength, was used to check the pH responsiveness. This hydrogel completely dissolved in acidic buffer solution (pH ~ 4.6, CH_3COOH-CH_3COONa) within few hours, emphasizing the supramolecular nature of the hydrogel, with co-ordination bonds being the dictating interaction. Here we have specifically engineered spatial structure with the hydrophobic α-methyl group (methacrylamide) to showcase the importance of hydrophobic interactions, as a gateway for second-order tuning of mechanical properties. The PMAI-Ni-4 was swelled at two different alkaline pH, 7.4 (phosphate buffer, physiological pH) and 9 ($NaCO_3$-$NaHCO_3$ buffer) (Fig. 3A). The swelling kinetics of the hydrogels revealed an intriguing swelling-deswelling phenomenon. Initially the polymer hydrogels swelled as a function of time because of the presence of ionic cross-links resulting in higher osmotic pressure. This was followed by deswelling until equilibrium was reached (Fig. 3A). UV–vis spectroscopic investigation of the dried gels (Fig. S4, Supporting Information) showed progressive red shift of the characteristic peaks with increasing pH, signifying that at higher pH, some of the imidazole units may be replaced by water in the co-ordination sphere of Ni^{2+}. This presumably exposes the hydrophobic methyl groups to the aqueous environment, leading to the formation of a more compact and rigid network structure with hydrophobic domains. In the process, the hydrogel expels water, resulting in de-swelling. On exposure to alkaline pH, the tensile stress–strain curve displayed a yield strain followed by necking and strain stiffening (Fig. 3B). Indeed, the hydrogel showed significant and progressive increase in stiffness with increase in pH (~121 MPa at pH 7.4 and ~155 MPa at pH 9) (Fig. 3C) compared to the as prepared hydrogel, while the stretchability decreased significantly (Fig. S5A, Supporting Information), revealing an extraordinary dependence of mechanical properties on pH (Fig. S5B,C, Supporting Information). A similar trend was also observed in compression experiments. The compressive modulus increased with increase in pH (Fig. 3D and E). The WAXD analysis did not show any crystalline peak for all the hydrogels, indicating their amorphous nature (Fig. S5D, Supporting Information). The corresponding Zn^{2+} based metallogel (PMAI-Zn-4) also showed a similar swelling-deswelling trend (Fig. S5E, Supporting Information), although the stiffness was lower than the PMAI-Ni-4 at respective pH (~63 MPa at pH 7.4 and ~77 MPa at pH 9) (Fig. 3C and Fig. S5F, Supporting Information). This trend is similar to that observed in the as prepared hydrogels (vide supra) and further illustrates the importance of metal–ligand exchange kinetics in dictating hydrogel mechanical properties. It was noted, similar to nickel-hydrogel, the strain at break decreased for PMAI-Zn-4 too at higher pH, but the extent of decrease was lower while higher gain in tensile strength ultimately led to increase in toughness (Fig. S5A-C,F, Supporting Information). Taken together, these results suggest a pH dependent transition of the hydrogel from a stiff rubbery to a stiff glassy state.

3.3. Dynamic mechanical analysis and oscillatory rheology of the hydrogels

The dynamic mechanical analysis revealed that an increase in pH resulted in the increase of compressive storage and loss modulus of both the PMAI-Ni-4 (Fig. 3F) and PMAI-Zn-4 (Fig. S6, Supporting Information) hydrogels, while when compared among themselves, the modulus values of PMAI-Zn-4 remained lower than the PMAI-Ni-4, consistent with the results of the tensile experiments. These observations reveal the importance of the metal–ligand interaction as the modulus values with the similar spatial structure are dictated by the temporal cross-links. Both the compressive storage and loss modulus decreased as the temperature was increased, indicating dynamic nature of the VIMZ-metal ion cross-links. The storage modulus remained higher than the loss modulus throughout the temperature range, implying that although the hydrogels became weaker, they remained stable even at higher temperature (Fig. 3F and Fig. S6, Supporting Information). Since hydrogels have a general tendency to dehydrate in air and this process can speed up during heating, the hydrogel samples were coated with silicone oil to minimize water loss during the variable temperature dynamic mechanical analysis. Additionally, the extent of water loss was investigated using thermogravimetric analysis at a heating rate of 5 °C min^{-1} (same as the variable temperature DMA experiment). The thermograms (Figs. S7A,B) reveal the rate of water loss for silicone oil coated hydrogels under these conditions was significantly slower than that of the uncoated hydrogels, and the water loss rates were also similar for the different hydrogels investigated. Next, shear rheology was used to

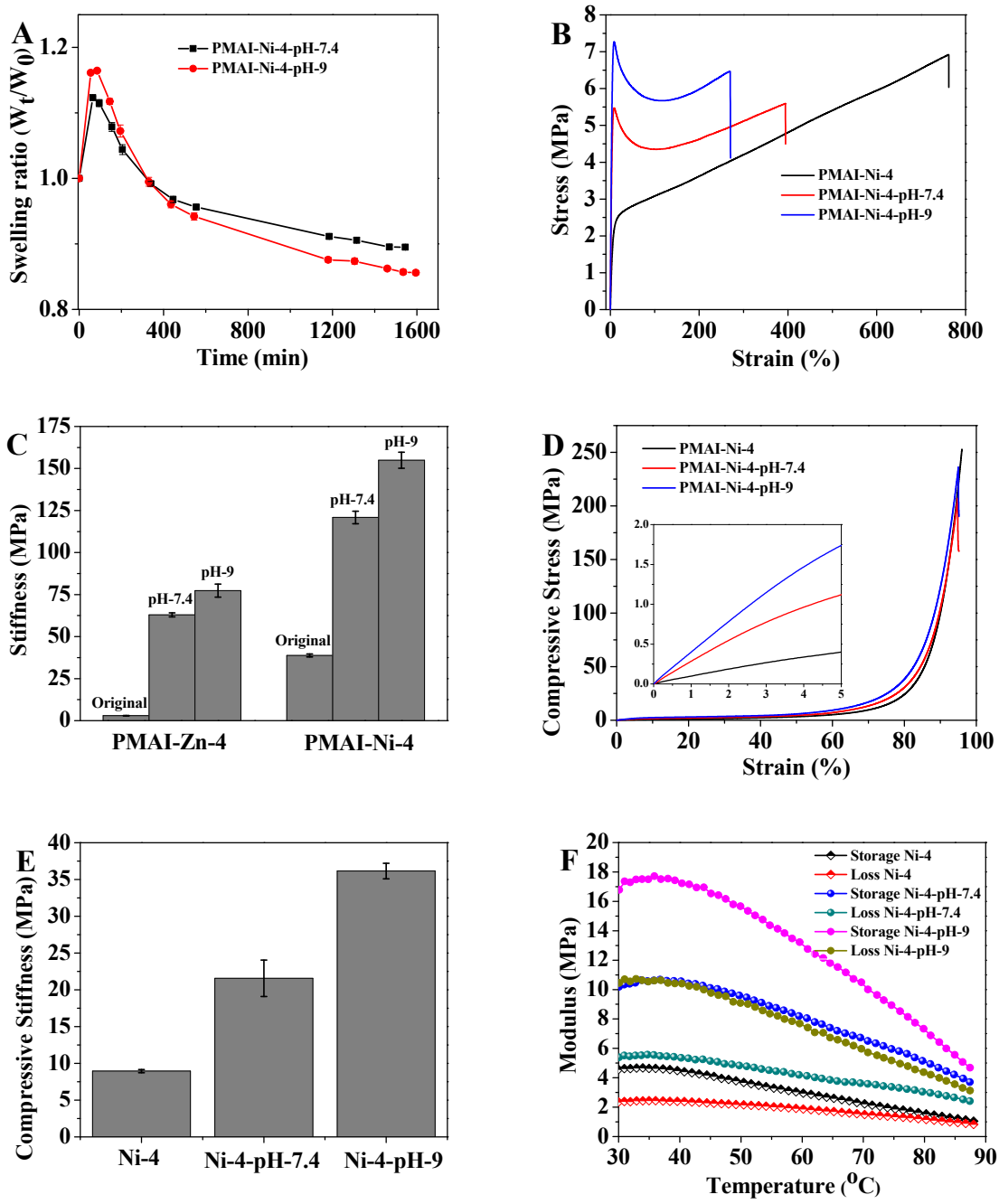

Fig. 3. A) The time dependency of swelling ratio for PMAI-Ni-4 at pH 7.4 and 9. B) Stress–strain curve of native PMAI-Ni-4 and PMAI-Ni-4 swelled at pH 7.4 and 9. C) Elastic modulus of PMAI-Zn-4, PMAI-Ni-4, swelled at pH 7.4 and 9. Compressive D) stress–strain curve and E) stiffness of PMAI-Ni-4 and PMAI-Ni-4 swelled at pH 7.4 and 9. F) Dynamic mechanical analysis: variation of storage and loss modulus of native PMAI-Ni-4 and PMAI-Ni-4 swelled at pH 7.4 and 9 with increase in temperature at a scan rate of 5 °C min^{-1}.

further evaluate the structural properties. The oscillatory strain sweep experiment (at a constant frequency of 1 Hz) of PMAI-Zn-4 (Fig. 4A) and PMAI-Ni-4 (Fig. 4B) shows the PMAI-Zn-4 have lower shear modulus values, further indicating the importance of metal–ligand exchange kinetics. PMAI-Zn-4 hydrogels revealed a significant decrease in breaking strain of the gel network after exposure to alkaline pH (Fig. 4A). This may be attributed to increased stiffness of the network at high pH, which in turn reduced the network flexibility. Frequency sweep rheology experiments (at 0.1% strain) showed significant frequency dependence of the storage and loss moduli for both PMAI-Zn-4 and PMAI-Ni-4 hydrogels, further confirming the reversible nature of the dynamic metal ion-imidazole cross-links (Fig. 4C, D) [54]. Step strain experiment was undertaken to investigate the self-healing capacity of these hydrogels. Accordingly, the hydrogels were subjected to consecutive cycles (180 s duration) of low strain (0.1% at 1 Hz) and large strain (100% at 1 Hz for as prepared Zn^{2+} hydrogels and 10% at 1 Hz for Ni^{2+} and Zn^{2+} hydrogels exposed to alkaline pH). At high strain, higher value of the shear loss modulus (G“) than the shear storage modulus (G’) indicated destruction of the gel network. When the low strain was subsequently applied, G’ quickly recovered its original value for all the hydrogels (Fig. 4E,F, and Fig. S8A,B, Supporting Information), suggesting the restoration of the network. The recyclable ultrafast recovery of modulus values indicates the importance of the dynamic dissociation and re-association of the metal ion-imidazole cross-links that endows these

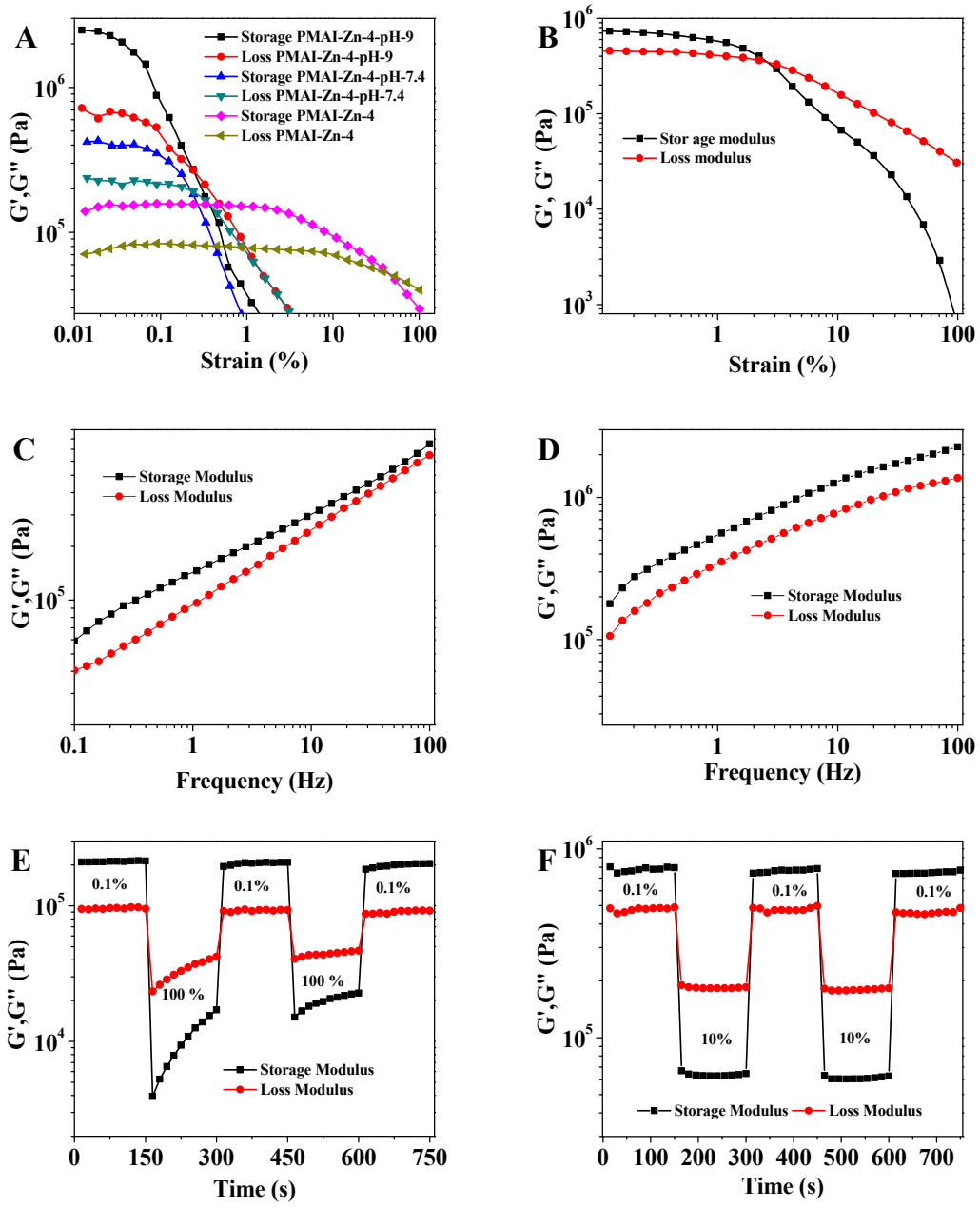

Fig. 4. Shear strain sweep of A) native PMAI-Zn-4 and PMAI-Zn-4 swelled at different pH and B) PMAI-Ni-4. Frequency sweep of C) PMAI-Zn-4 and D) PMAI-Ni-4. Intrinsic self-healing experiment (Thixotropic) of E) PMAI-Zn-4, F) PMAI-Ni-4 at constant frequency of 1 Hz and temperature 25 °C.

hydrogels the ability to recover mechanical properties after damage. Hence, from the above result, we have seen the metal–ligand interaction not only shows stimuli responsiveness property but it can be used as a "gateway" for greater tailor-ability.

3.4. Shape memory property and structural application of the hydrogels

The ultra-stiffness of PMAI-Ni-4 and its temperature-dependent mechanical property (DMA) (Fig. 3F), along with the reversible nature of temporal interaction with excellent recovery (Fig. 4D, F) suggests possible shape-memory behaviour of these hydrogels. The PMAI-Ni-4 hydrogel in rectangular shape (permanent shape) was twisted to the helix form (temporary shape) at room temperature and then fixed by cooling it to 10 °C and keeping at this temperature for 30 min. The shape recovery was monitored by immersing the hydrogel in a silicone oil bath to prevent water removal at elevated temperature (50 °C). The hydrogel sample regained its original shape within few seconds (Fig. 5A-C and video S2, Supporting Information), manifesting the good shape memory property.

The outstanding mechanical properties endowed PMAI-M−X series suitable for applications as robust structural materials. For example, a rectangular strip of the PMAI-Ni-4 hydrogel (thickness ~1 mm and width ~6 mm) can lift a weight of 4 kg (Fig. S9A, Supporting Information), and the same equilibrated at pH 9 can lift a weight of 7 kg (Fig. 5D). The PMAI-Zn-4 hydrogel equilibrated at pH 9 can lift a load of 6 kg (Fig. S9B, Supporting Information). A rectangular sheet (thickness ~1 mm, width ~20 mm) of PMAI-Ni-4 equilibrated at pH 9 was able to bear a weight of ~125 g without collapse (Fig. 5E) because of high stiffness. Moreover, four cylinders (diameter ~24 mm) of PMAI-Ni-4 can carry a person (weight ~55 kg) without any visible deformation (Fig. 5F and video S3, Supporting Information). Considering the outstanding mechanical properties, a glass vial (containing Rhodamine-B aqueous

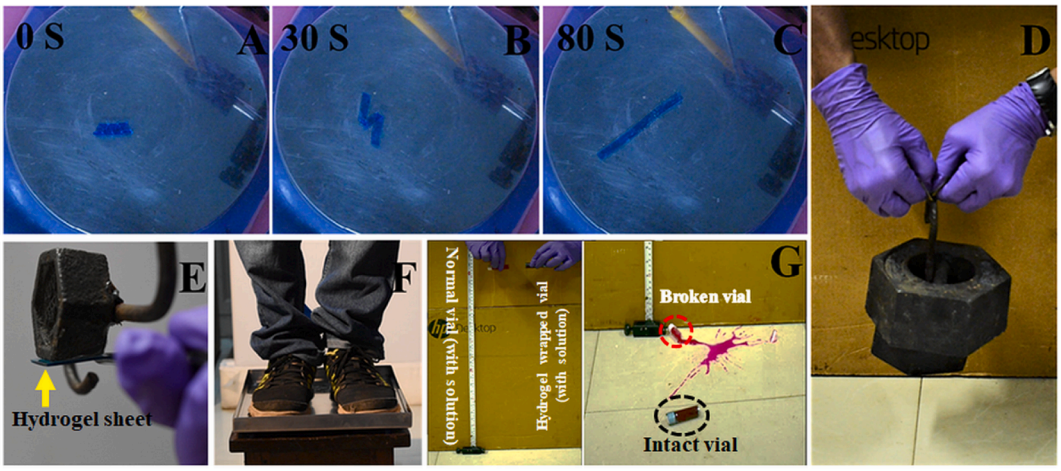

Fig. 5. Photographs: Fast temperature dependent Shape memory behavior of PMAI-Ni-4 at A) 0, B) 30, C) 80 s at 50 °C inside silicone oil. D) A Strip of PMAI-Ni-4-pH 9 (thickness 1 mm and width 6 mm) lifting 7 kg weight. . E) A strip of PMAI-Ni-4-pH-9 can handle a weight of 125 g, showcasing its great stiffness; F) Four Cylinders of PMAI-Ni-4 can take a weight of a person (55 kg) without any collapse and G) Protection of fragile item (glass vial with red solution).

solution) was wrapped with a sheet of PMAI-Ni-4 (thickness ~1 mm) and dropped from a height of 2 ft. along with a similar unwrapped vial. The hydrogel wrapped vial remained intact while the bare vial was shattered into pieces (Fig. 5G and Video S4, Supporting Information).

3.5. Ionic conductivity of the hydrogels

The presence of dynamic metal–ligand motifs in these hydrogels indicates that these materials should be ionically conducting. Generally, the improvement in mechanical properties of the polymer network is associated with stronger co-ordination of the metal ion with the ligand presented by the polymer backbone, resulting in restricted segmental motion, decreased mobility of the metal ions, and reduced ionic conductivity. Hence the ion-polymer interaction with improved mechanical properties (lower segmental motion) remains at the core of trade-off between ion concentration and mobility [55]. The PMAI-Ni-X hydrogels showed an increase in ionic conductivity with increasing Ni^{2+} concentration (from 5.72 mS cm^{-1} in PMAI-Ni-6 to 17.37 mS cm^{-1} in PMAI-Ni-2, see Table S2, Supporting Information). This observation can be attributed to the simultaneous increase in the number of charge carriers as well as the polymer segmental motion (because of decrease in hydrogel stiffness with decreasing L/M ratio, vide supra), which should synergistically favour ionic conductivity. As PMAI-Ni-2 showed the highest conductivity in the PMAI-Ni-X hydrogel series, we checked the corresponding PMAI-Zn-2 hydrogel to evaluate the effect of metal–ligand dynamics on ionic conductivity. The ionic conductivity of PMAI-Zn-2 hydrogel was significantly lower (5.71 mS cm^{-1}) than that of PMAI-Ni-2 (17.37 mS cm^{-1}) (Table S2, Supporting Information), despite having faster relaxation of imidazole-Zn^{2+} cross-links. This observation can be attributed to the fact that the ionic conductivity observed is the overall conductivity imparted by both cation and anion and depends on the salt used. The $ZnSO_4$-gel polymer electrolyte for zinc-based battery has been reported to show ionic conductivity of 5.56 mS cm^{-1} for $ZnSO_4$/Polyacrylamide and 5.90 mS cm^{-1} for $ZnSO_4$/ cellulose film [56]. The observed ionic conductivity (5.71 mS cm^{-1}) for our PMAI-Zn-2 hydrogel is consistent with these literature reports. The ionic conductivity of these hydrogels is higher than other reported metal–ligand based hydrogel [51,57], and of the same order of magnitude to the conductivity observed in hydrogels with additional salts [7,11,58]. With these hydrogels, we have chosen to demonstrate two kinds of ionotronics applications: (1) tactile sensing, which deals with mechanics dependent conductivity, and (2) as a solid electrolyte for compressible supercapacitors where not only high conductivity but also the nature of conducting ions play an important role. Primarily, PMAI-Ni-2 and PMAI-Zn-2 were chosen due to their better conductivity, and PMAI-Zn-4 was taken for comparison. Before proceeding with these experiments, the self-recovery property of these hydrogels under tension and compression, along with their self-healing ability were investigated in detail to evaluate their suitability for these applications.

3.6. Self-recovery and fatigue experiments

The hydrogels were subjected to tensile loading–unloading cycles up to 100% strain. All the hydrogels showed some amount of residual strain after completion of the first cycle (Fig. 6A and Fig. S10A,B, Supporting Information). The dissipated energy accounted for about 50–70% of the total work, suggesting a prominent role of the sacrificial VIMZ-M^{2+} cross-links as energy dissipating motifs (Fig. 6B). When the hydrogels were subjected to the second cycle after a resting period of 2 min, almost quantitative recovery of the original dissipated energy (hysteresis area) was observed (Fig. 6C), demonstrating their extraordinary recovery property. The excellent self-recovery performance of the hydrogels prompted us to investigate their anti-fatigue characteristics. Accordingly, the PMAI-Zn-2 hydrogel was subjected to 10 consecutive loading–unloading cycles up to 100% strain. It can be observed that from the second cycle onwards, the area under the hysteresis curve decreased substantially (Fig. 6D), due to the internal damage caused and the inability of the hydrogels to recover the reversible bonds due to repetition of the cycles without rest. When the second set of 10 cycles were performed after resting the sample for only 2 min., the PMAI-Zn-2 recovered ~89% of the original dissipated energy when the hysteresis areas of the first cycles were compared (Fig. 6E and 6F). Similar results were obtained for PMAI-Zn-4 and PMAI-Ni-2 hydrogels (Fig. S11A-F, Supporting Information). It can be noted that some of the hydrogels recovered more than 100% of the original stress, which is possibly a consequence of breaking and rejoining of imidazole-metal ion cross-links at new accessible sites leading to stronger network, similar to previous observations by our group and others [20]. These results indicate robust fatigue resistance characteristics of this class of hydrogel materials under tensile loading. The hydrogels were then subjected to compressive loading–unloading cycle up to 50% strain. When the second loading–unloading cycle was executed after resting the samples for only 2 min, PMAI-Zn-2, PMAI-Zn-4, and PMAI-Ni-2 hydrogels recovered ~80–90% of the original dissipated energy (hysteresis Area) and more than 95% of compressive strength, showcasing their excellent recovery property under compression at ambient condition (Fig. 7A-D). Although these experiments demonstrate the robust mechanical properties of the hydrogels, for day to day use the material can develop micro-cracks or

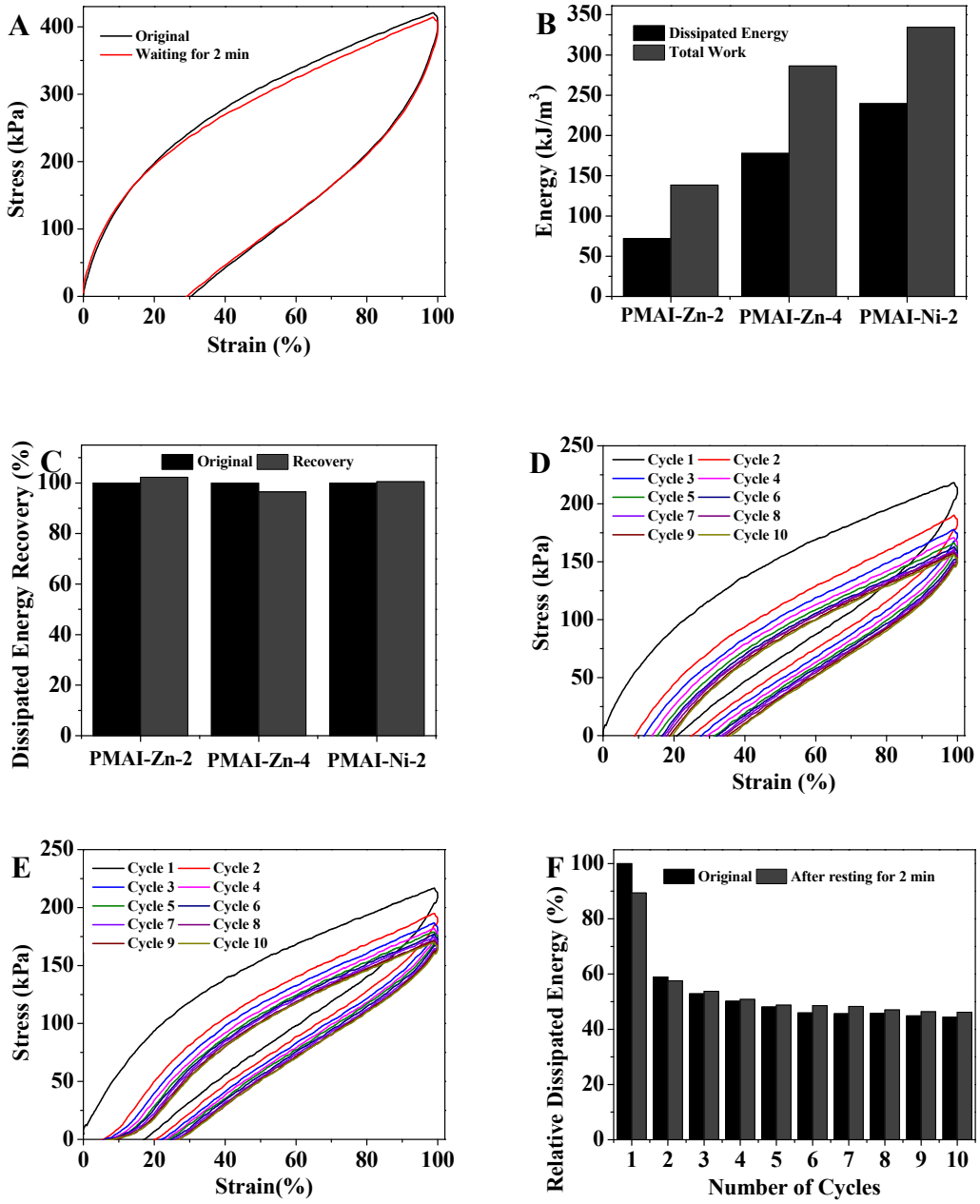

Fig. 6. Tensile cyclic loading–unloading curve of A) PMAI-Zn-4, B) dissipated energy (hysteresis area) with total work (area under loading curve) and C) recovery of dissipated energy of PMAI-Zn-2, PMAI-Zn-4 and PMAI-Ni-2 respectively at 100% strain. Ten successive fatigue cycle at 100% strain of D) PMAI-Zn-2, E) PMAI-Zn-2 after resting for 2 min F) Relative dissipated energy of PMAI-Zn-2 and recovered PMAI-Zn-2 after resting for 2 min.

cuts, which can lead to structural failure. As observed from step strain rheology experiment (vide supra, Fig. 4E-F), after breakage of the network, these hydrogels are able to recover their storage and loss modulus values within seconds. Self-healing of the hydrogels was also also evident through tensile experiment. For example, the PMAI-Zn-2 hydrogel was cut into two pieces and gently pressed together for 4 h at 37 °C. This hydrogel sample, when subjected to tensile test, could still be stretched to more than 200% strain with a recovery of ~87% of its original stiffness (Fig. S12, Supporting Information). Taken together, these results demonstrate that this class of fully physically cross-linked self-healable hydrogels show excellent self-recovery and anti-fatigue properties.

3.7. Flexible resistive strain sensor

The metallo-hydrogels showed colour depending on the co-ordination bond (metal ion) present in the hydrogel. While the PMAI-Ni-2 shows bluish-green colour the PMAI-Zn-2/4 is colourless, although all the hydrogels are optically transparent (Fig. 8A). The colourless transparent nature of the zinc variant gives it an advantage over the coloured metal–ligand based hydrogels, as it can be utilized for ionotronics devices [59,60]. The imidazole-zinc complex is also prevalent in biological materials. Hence, the Zn^{2+} based hydrogels were chosen to demonstrate sensor applications. When the PMAI-Zn-4 hydrogel was connected with a battery (9 V), it was able to conduct electricity to light a LED bulb. Upon stretching the hydrogel, the intensity of light diminished, indicating the increase in resistance. The subsequent hydrogel recovery led to brightened light intensity,

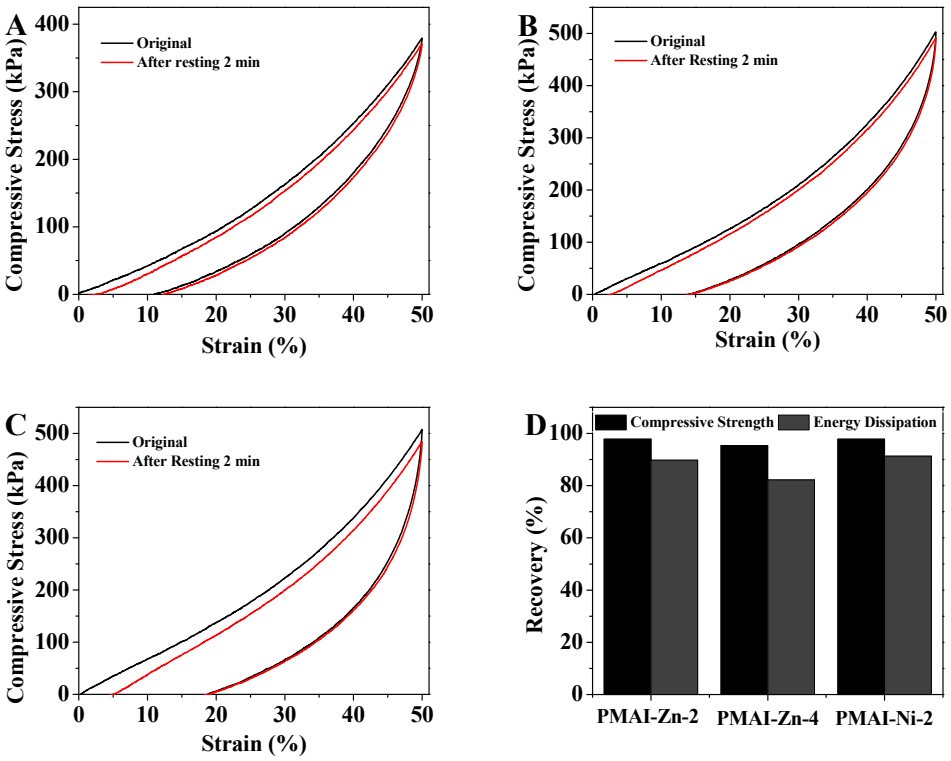

Fig. 7. Compressive cyclic loading–unloading curve of A) PMAI-Zn-2, B) PMAI-Ni-2 and C) PMAI-Zn-4. D) Percentage of recovery of dissipation of energy and compressive strength after resting the PMAI-Zn-2,4 and PMAI-Ni-2 hydrogels for 2 min.

indicating the suitability of the hydrogel for sensory applications (Fig. 8B). For quantitative evaluation, both resistive and capacitive sensors were prepared (thickness ~1 mm) from the above conductive gels. The resistive sensors were prepared by sandwiching the conductive gel in between two commercially available VHB-4910 adhesive dielectric tapes (to prevent the water evaporation) (Fig. S13A, Supporting Information), The effectiveness of the PMAI-Zn-4 based stretchable resistive sensor was checked by plotting the change in relative resistance as a function of tensile strain (Fig. 8C), where the relative resistance change is defined as $(R_i - R_0)/R_0$, where the R_0 and R_i were the resistance at 0% strain and different strains respectively. The rate of change in relative resistance increased with strain percentage and the relative resistance change reached a value of nearly 44 at 200% strain, which shows that the hydrogel is very sensitive towards applied strain. Gauge factor, GF (relative resistance change divided by applied strain), is used to predict the sensitivity of the sensors [61]. The gauge factor for this resistive sensor was ~11 and 22 at 100 and 200% strain respectively (Fig. 8D), which is much higher than that of piezoresistive electronic strain sensors (GF 0.82 at 0 to 40% and 0.06 at 60 to 200% strain) [62], SWCNT/hydrogel (GF 0.25 at 100% strain) [61], DN hydrogel (GF 0.23 at 100% strain) [63], P(AM-co-AA)/CS DN ionic hydrogel (GF ~2 at 100% and ~2.5 at 200% strain) [7], and conventional metal gauges (GF 2 at 5% maximum strain) [64]. We demonstrated the application of this resistive sensor as a wearable strain sensor to monitor the movement of a finger (Fig. 8E and video S4, Supporting Information). Relative to the straight finger, the resistance increases when the finger is bent because of stretching of the hydrogel. As expected, the relative resistance change (%) was very high due to higher sensitivity (high gauge factor), which makes it an excellent sensor to monitor human motion.

3.8. Flexible capacitive pressure sensor

In order to prepare a capacitive sensor, the dielectric (VHB) was sandwiched between two conductive gel layers (thickness- 1 mm) followed by a layer of VHB tape to prevent water removal (Fig. S13B, Supporting Information). In the present work, two capacitive pressure sensors were prepared from PMAI-Zn-2 and PMAI-Zn-4 hydrogels for comparison, and relative change of capacitance $[(C_i - C_0)/C_0$, C_i and C_0 are capacitance at loads of different weights and at zero load, respectively] was measured as a function of weight (Fig. 8F). For both the hydrogels, the relative capacitance change (%) increased nearly linearly with increase in weight. However, the extent of relative capacitance increase was higher for PMAI-Zn-2 than PMAI-Zn-4. As observed from the compression experiments (vide supra, Fig. 2A and C), the compressive modulus (stiffness) of the PMAI-Zn-2 hydrogel (0.433 ± 0.01 MPa) is significantly lower than that of the PMAI-Zn-4 hydrogel (0.805 ± 0.028) MPa. These data clearly suggest that the extent of deformation will be significantly higher for PMAI-Zn-2 than PMAI-Zn-4 for the same compressive load and as a consequence, the change in relative capacitance is also higher (the decrease in thickness of the dielectric layer is same for both the gels at same applied load). Subsequently, the PMAI-Zn-2 and 4 based sensors were used to monitor the pressure applied by hand. Fig. 8G and Fig. S13C show clear transition in percentage relative capacitance change with good repeatability.

3.9. Fabrication of compressible supercapacitor

Using PMAI-Ni-2 and PMAI-Zn-2 hydrogels as electrolytes, soft and deformable supercapacitor devices were prepared by sandwiching the respective hydrogels between two activated carbon coated graphite sheet electrodes. It should be noted that unlike other literature reports, no extra salt such as KCl, NaCl, and Na_2SO_4 was added to increase the conductivity [11]. Hence, solely the dynamic metal–ligand cross-links and unco-ordinated ions play the critical role. The electrochemical performance of the supercapacitor was evaluated by cyclic voltammetry (CV), galvanostatic charge–discharge (GCD) and electrochemical impedance spectroscopy (EIS) measurement. The CV at the potential window of 0 to 0.8 V at scan rates ranging from 5 to 100 mV s^{-1} showed nearly symmetrical quasi-rectangular curves (Fig. 9A and Fig. S14A, Supporting Information), which is typical for electrochemical double-

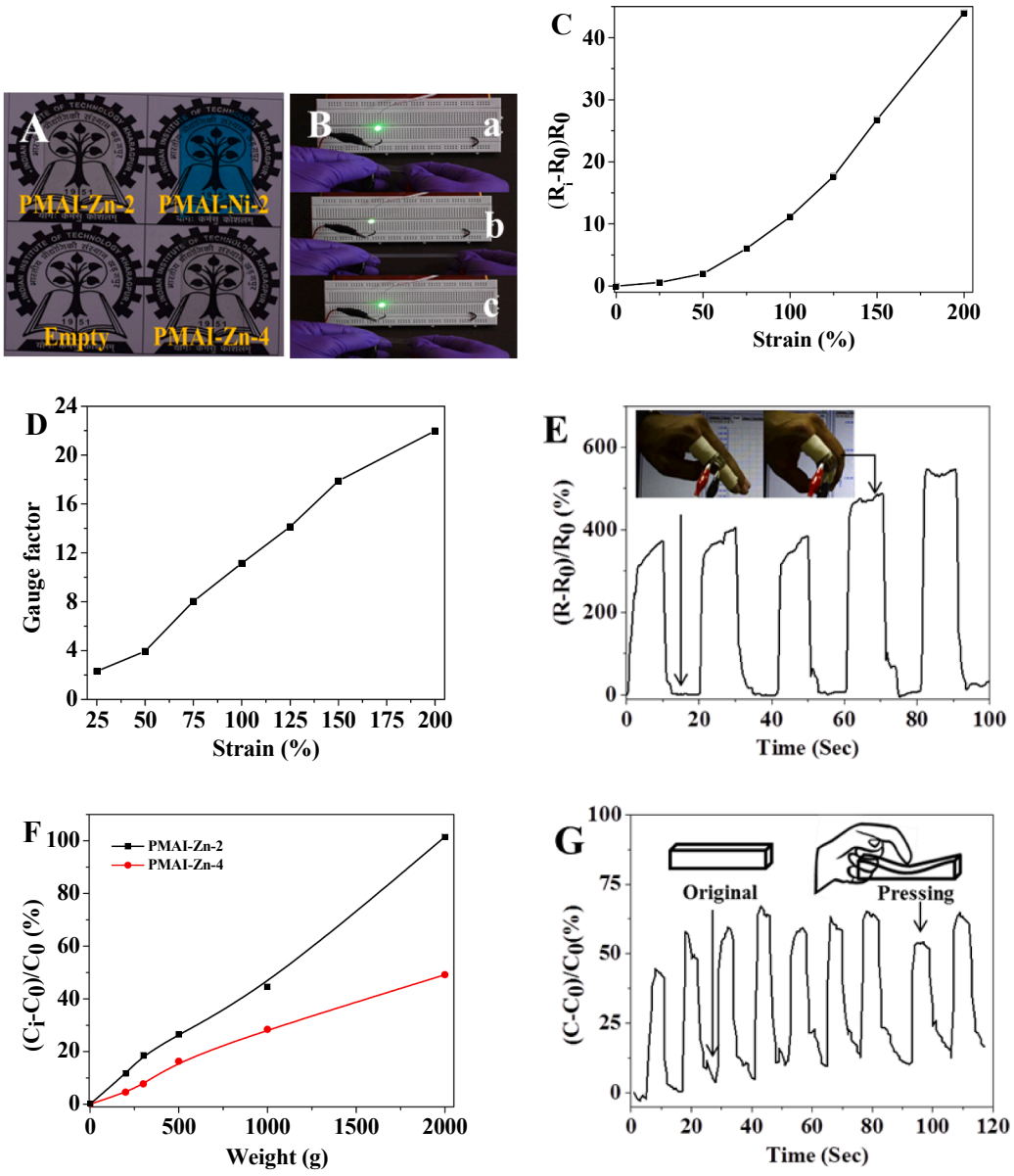

Fig. 8. A) Optical transparency of PMAI-Zn-2, PMAI-Zn-4 and PMAI-Ni-2. B) Lighting of LED a) original b) under stretch intensity goes down c) upon removal of strain intensity gets back. C) Change of relative resistance as a function of strain, D) gauge factor and E) monitoring of movement of finger using PMAI-Zn-4 hydrogel based resistive sensor. F) Change of relative capacitance of PMAI-Zn-2 and of PMAI-Zn-4, G) pressure sensing using PMAI-Zn-2 hydrogel based capacitive sensor.

layer capacitor (EDLC) suggesting that the hydrogels can be used as an electrolyte. GCD profiles were taken at current density ranging from 20 mA g^{-1} to 100 mA g^{-1} and the specific capacitance was calculated from the GCD curves. PMAI-Ni-2 and PMAI-Zn-2 showed specific capacitance of 98.9F g^{-1} and 70F g^{-1}, respectively at the current density of 20 mA g^{-1} (Fig. 9B-C and Fig. S14B,C, Supporting Information). Considering the excellent compressive properties of the electrolyte, the capacitance behaviour of the supercapacitor was further investigated by recording the CV under different loads (weight). Owing to high compressive strength of the hydrogels, the capacitor can withstand a heavy load of 2000 g cm^{-2}, which accounts for ~3120 and 2932 fold weight of the whole capacitor for PMAI-Ni-2 and PMAI-Zn-2 respectively (Fig. 9D) [12] .The nature of CV curves (Fig. S14D,E, Supporting Information) remains same even at this huge applied load, suggesting the supercapacitor can work well under extreme load. The specific capacitance value initially increased with an increase in weight (load), reaching ~99% and 112% at 1000 g cm^{-2}, which accounts for ~1560 and 1466 fold weight of the whole supercapacitor for PMAI-Ni-2 and PMAI-Zn-2 respectively. Further increase in weight became detrimental for PMAI-Ni-2 based device although the PMAI-Zn-2 based device was able to maintain its electrochemical performance (Fig. 9D). The increase of specific capacitance with increasing load may be attributed to the compression under the load, which leads to a thinner electrolyte. The EIS data of both the supercapacitors before and after the compression are shown in Fig. S14F. The EIS plots show a compressed semicircle and straight line in the high and low frequency regime, respectively. The diameter of semicircle appeared to be decreased after compression, which suggests lower charge transfer resistance leading to higher specific capacitance value. Following the demonstration of stable electrochemical performance under high load, the PMAI-Zn-2 based supercapacitor was examined by CV for 1000 cycles, and the specific capacitance retention remained close to 100% (Fig. S15, Supporting Information). Collectively from the above results, it can be understood that this class of hydrogels can be utilized as electrolytes to produce compressible supercapacitors. The intrinsic stretchability with good self-healing and self-recovery capability makes these materials potential

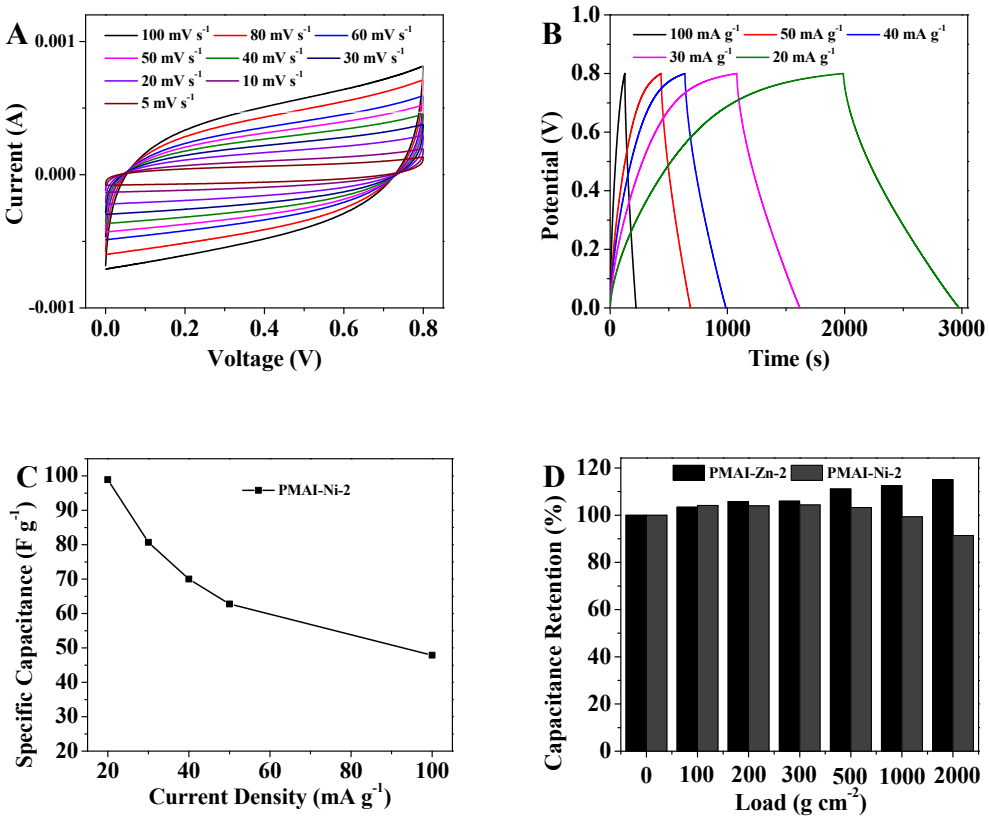

Fig. 9. A) Cyclic voltammetry at different scan rate B) Charge-discharge, at different current density and dependency of specific capacitance C) as a function of current density, for PMAI-Ni-2 hydrogel based EDLC. D) Relative change in specific capacitance of PMAI-Zn-2 and PMAI-Ni-2 as a function of applied weight.

candidate as an electrolyte for stretchable supercapacitor and battery, which will be explored subsequently.

4. Conclusions

In summary, we have prepared fully physically cross-linked metallo-hydrogels poly(metharylamide-co-vinylimidazole)-M^{2+} (M = Ni, Zn) via simple one-pot synthetic procedure. By effectively controlling the L/M ratio and metal–ligand exchange kinetics - whilst the total monomer concentrations and co-monomer ratio were kept constant - a wide spectrum of mechanical properties was achieved (compressive strength-103 to 247 MPa at 96% strain and compressive stiffness of ~0.434 to 8.95 MPa; elastic modulus ~0.73 to 40 MPa; tensile strength ~0.55 to 6.8 MPa; toughness ~1 to 35.88 MJ m^{-3}). The combination of pH-sensitive metal–ligand cross-links and hydrophobic methyl group in the backbone were utilized for further tuning of hydrogel mechanial properties, to obtain elastic modulus up to 155 MPa (and compressive modulus up to 36 MPa). The hydrogels showed fast self-recovery and robust anti-fatigue characteristics, along with shape memory and self-healing properties. Furthermore, applications of these hydrogels were demonstrated as highly sensitive (Gauge factor 11 at 100% and 22 at 200%) resistive sensor for human motion detection and capacitive sensor for pressure sensing, and as a solid electrolyte to fabricate highly compressible supercapacitors. Hence this work demonstrates very simple and effective strategy to control the mechanical and functional properties of hydrogel materials to cater the needs of specific applications.

Declaration of Competing Interest

The authors declare that they have no known competing financial interests or personal relationships that could have appeared to influence the work reported in this paper.

Acknowledgements

The authors thank Mr. Arijit Ghorai for helping in measurement of ionic conductivity, Mr. Suman Kumar Si and Mr. Sarbaranjan Paria for helping to measure capacitance. The authors also thank Mr. Sourav Das and Mr. Shaikh Parwaiz for helping to handle Keithley 4200 SCS machine and CHI 760D electrochemical workstation respectively.

K.S. acknowledges DST-SERB, India for financial supports (Grant No. EEQ/2016/000712 and ECR/2016/002018). K.S. also acknowledges UGC for UGC-BSR Research Start-Up Grant (F.30-363/2017(BSR), Dt-08/08/2017) and CU for UPE-II Nanofabrication project fund (UGC/166/UPE-II, Dt- 03/04/2017) for financial support. R.K.D. acknowledges financial support from SERB, India (Grant No. ECR/2017/000539) and the IIT Kharagpur (Initiation Grant No. IIT/SRIC/ISIRD/2016-2017).

Appendix A. Supplementary data

Supplementary data to this article can be found online at https://doi.org/10.1016/j.cej.2021.129528.

References

[1] B.V. Slaughter, S.S. Khurshid, O.Z. Fisher, A. Khademhosseini, N.A. Peppas, Hydrogels in Regenerative Medicine, Adv. Mater. 21 (32-33) (2009) 3307–3329, https://doi.org/10.1002/adma.200802106.

[2] M. Liu, X. Zeng, C. Ma, H. Yi, Z. Ali, X. Mou, S. Li, Y. Deng, N. He, Injectable hydrogels for cartilage and bone tissue engineering, Bone Res. 5 (1) (2017), https://doi.org/10.1038/boneres.2017.14.

[3] J. Kopecek, Hydrogels: From soft contact lenses and implants to self-assembled nanomaterials: Highlight, J. Polym. Sci. A Polym. Chem. 47 (22) (2009) 5929–5946, https://doi.org/10.1002/pola.23607.

[4] L. Xu, L. Qiu, Y. Sheng, Y. Sun, L. Deng, X. Li, M. Bradley, R. Zhang, Biodegradable pH-responsive hydrogels for controlled dual-drug release, J. Mater. Chem. B 6 (3) (2018) 510–517, https://doi.org/10.1039/C7TB01851G.

[5] M. Rizwan, R. Yahya, A. Hassan, M. Yar, A. Azzahari, V. Selvanathan, F. Sonsudin, C. Abouloula, pH Sensitive Hydrogels in Drug Delivery: Brief History, Properties, Swelling, and Release Mechanism, Material Selection and Applications, Polymers (Basel). 9 (2017) 137. https://doi.org/10.3390/polym9040137.

[6] Z. Lei, P. Wu, A supramolecular biomimetic skin combining a wide spectrum of mechanical properties and multiple sensory capabilities, Nat. Commun. 9 (2018) 1–7, https://doi.org/10.1038/s41467-018-03456-w.

[7] Y. Liang, L. Ye, X. Sun, Q. Lv, H. Liang, Tough and stretchable dual ionically cross-linked hydrogel with high conductivity and fast recovery property for high-performance flexible sensors, ACS Appl. Mater. Interfaces 12 (1) (2020) 1577–1587, https://doi.org/10.1021/acsami.9b18796.s001.

[8] Z. Wang, H. Zhou, J. Lai, B.o. Yan, H. Liu, X. Jin, A. Ma, G. Zhang, W. Zhao, W. Chen, Extremely stretchable and electrically conductive hydrogels with dually synergistic networks for wearable strain sensors, J. Mater. Chem. C 6 (34) (2018) 9200–9207, https://doi.org/10.1039/C8TC02505C.

[9] X. Le, W. Lu, J. Zhang, T. Chen, Recent Progress in Biomimetic Anisotropic Hydrogel Actuators, Adv. Sci. 6 (5) (2019) 1801584, https://doi.org/10.1002/advs.201801584.

[10] Y. Lee, W.J. Song, J.-Y. Sun, Hydrogel soft robotics, Mater. Today Phys. 15 (2020) 100258, https://doi.org/10.1016/j.mtphys.2020.100258.

[11] L. Xin Dai, W. Zhang, L. Sun, X. Huo Wang, W. Jiang, Z. Wen Zhu, H. Bin Zhang, C. Cai Yang, J. Tang, Highly stretchable and compressible self-healing P(AA-co-AAm)/CoCl2 hydrogel electrolyte for flexible supercapacitors, ChemElectroChem. 6 (2019) 467–472, https://doi.org/10.1002/celc.201801281.

[12] Y. Huang, M. Zhong, F. Shi, X. Liu, Z. Tang, Y. Wang, Y. Huang, H. Hou, X. Xie, C. Zhi, An intrinsically stretchable and compressible supercapacitor containing a polyacrylamide hydrogel electrolyte, Angew. Chem. Int. Ed. 56 (31) (2017) 9141–9145, https://doi.org/10.1002/anie.201705212.

[13] Y. Wang, J. Liu, Y. Feng, N. Nie, M. Hu, J. Wang, G. Pan, J. Zhang, Y. Huang, An intrinsically stretchable and compressible Zn–air battery, Chem. Commun. 56 (35) (2020) 4793–4796, https://doi.org/10.1039/D0CC00823K.

[14] J. Liu, M. Hu, J. Wang, N. Nie, Y. Wang, Y. Wang, J. Zhang, Y. Huang, An intrinsically 400% stretchable and 50% compressible NiCo//Zn battery, Nano Energy 58 (2019) 338–346, https://doi.org/10.1016/j.nanoen.2019.01.028.

[15] J.P. Gong, Y. Katsuyama, T. Kurokawa, Y. Osada, Double-network hydrogels with extremely high mechanical strength, Adv. Mater. 15 (2003) 1155–1158, https://doi.org/10.1002/adma.200304907.

[16] J.-Y. Sun, X. Zhao, W.R.K. Illeperuma, O. Chaudhuri, K.H. Oh, D.J. Mooney, J. J. Vlassak, Z. Suo, Highly stretchable and tough hydrogels, Nature 489 (7414) (2012) 133–136, https://doi.org/10.1038/nature11409.

[17] J. Zheng, C. Zhao, L. Zhu, Q. Chen, Q. Wang, A. Robust, One-pot synthesis of highly mechanical and recoverable double network hydrogels using thermoreversible sol-gel polysaccharide, Adv. Mater. 25 (2013) 4171–4176, https://doi.org/10.1002/adma.201300817.

[18] Q. Chen, L. Zhu, H. Chen, H. Yan, L. Huang, J. Yang, J. Zheng, A novel design strategy for fully physically linked double network hydrogels with tough, fatigue resistant, and self-healing properties, Adv. Funct. Mater. 25 (10) (2015) 1598–1607, https://doi.org/10.1002/adfm.201404357.

[19] P. Lin, S. Ma, X. Wang, F. Zhou, Molecularly engineered dual-crosslinked hydrogel with ultrahigh mechanical strength, toughness, and good self-recovery, Adv. Mater. 27 (12) (2015) 2054–2059, https://doi.org/10.1002/adma.201405022.

[20] A. Dutta, R.K. Das, Dual cross-linked hydrogels with high strength, toughness, and rapid self-recovery using dynamic metal–ligand interactions, Macromol. Mater. Eng. 304 (8) (2019) 1900195, https://doi.org/10.1002/mame.201900195.

[21] K. Haraguchi, T. Takehisa, Nanocomposite hydrogels: A unique organic-inorganic network structure with extraordinary mechanical, optical, and swelling/De-swelling properties, Adv. Mater. 14 (2002) 1120, https://doi.org/10.1002/1521-4095(20020816)14:16<1120::aid-adma1120>3.0.co;2-9.

[22] J. Yang, S. Liu, Y. Xiao, G. Gao, Y. Sun, Q. Guo, J. Wu, J. Fu, Multi-responsive nanocomposite hydrogels with high strength and toughness, J. Mater. Chem. B 4 (9) (2016) 1733–1739, https://doi.org/10.1039/C6TB00135A.

[23] Q. Li, D.G. Barrett, P.B. Messersmith, N. Holten-Andersen, Controlling hydrogel mechanics via bio-inspired polymer-nanoparticle bond dynamics, ACS Nano. 10 (2016) 1317–1324, https://doi.org/10.1021/acsnano.5b06692.

[24] X. Zhao, Multi-scale multi-mechanism design of tough hydrogels: building dissipation into stretchy networks, Soft Matter 10 (5) (2014) 672–687, https://doi.org/10.1039/C3SM52272E.

[25] N. Rauner, M. Meuris, M. Zoric, J.C. Tiller, Enzymatic mineralization generates ultrastiff and tough hydrogels with tunable mechanics, Nature 543 (7645) (2017) 407–410, https://doi.org/10.1038/nature21392.

[26] M.T.I. Mredha, Y.Z. Guo, T. Nonoyama, T. Nakajima, T. Kurokawa, J.P. Gong, A facile method to fabricate anisotropic hydrogels with perfectly aligned hierarchical fibrous structures, Adv. Mater. 30 (9) (2018) 1704937, https://doi.org/10.1002/adma.201704937.

[27] X. Hu, M. Vatankhah-Varnoosfaderani, J. Zhou, Q. Li, S.S. Sheiko, Weak hydrogen bonding enables hard, strong, tough, and elastic hydrogels, Adv. Mater. 27 (43) (2015) 6899–6905, https://doi.org/10.1002/adma.201503724.

[28] Y.J. Wang, X.N. Zhang, Y. Song, Y. Zhao, L.i. Chen, F. Su, L. Li, Z.L. Wu, Q. Zheng, Ultrastiff and tough supramolecular hydrogels with a dense and robust hydrogen bond network, Chem. Mater. 31 (4) (2019) 1430–1440, https://doi.org/10.1021/acs.chemmater.8b05262.s001.

[29] X.N. Zhang, Y.J. Wang, S. Sun, L. Hou, P. Wu, Z.L. Wu, Q. Zheng, A tough and stiff hydrogel with tunable water content and mechanical properties based on the synergistic effect of hydrogen bonding and hydrophobic interaction, Macromolecules 51 (20) (2018) 8136–8146, https://doi.org/10.1021/acs.macromol.8b01496.s001.

[30] C. Fan, B. Liu, Z. Xu, C. Cui, T. Wu, Y. Yang, D. Zhang, M. Xiao, Z. Zhang, W. Liu, Polymerization of: N -acryloylsemicarbazide: A facile and versatile strategy to tailor-make highly stiff and tough hydrogels, Mater. Horizons. 7 (2020) 1160–1170, https://doi.org/10.1039/c9mh01844a.

[31] J. Cao, J. Li, Y. Chen, L. Zhang, J. Zhou, Dual physical crosslinking strategy to construct moldable hydrogels with ultrahigh strength and toughness, Adv. Funct. Mater. 28 (23) (2018) 1800739, https://doi.org/10.1002/adfm.201800739.

[32] Y. Liang, J. Xue, B. Du, J. Nie, Ultrastiff, tough, and healable ionic–hydrogen bond cross-linked hydrogels and their uses as building blocks to construct complex hydrogel structures, ACS Appl. Mater. Interfaces 11 (5) (2019) 5441–5454, https://doi.org/10.1021/acsami.8b20520.s003.

[33] S.C. Grindy, R. Learsch, D. Mozhdehi, J. Cheng, D.G. Barrett, Z. Guan, P. B. Messersmith, N. Holten-Andersen, Control of hierarchical polymer mechanics with bioinspired metal-coordination dynamics, Nature Mater 14 (12) (2015) 1210–1216, https://doi.org/10.1038/nmat4401.

[34] D. Mozhdehi, J.A. Neal, S.C. Grindy, Y. Cordeau, S. Ayala, N. Holten-Andersen, Z. Guan, Tuning dynamic mechanical response in metallopolymer networks through simultaneous control of structural and temporal properties of the networks, Macromolecules 49 (17) (2016) 6310–6321, https://doi.org/10.1021/acs.macromol.6b01626.s001.

[35] S. Xia, S. Song, F. Jia, G. Gao, A flexible, adhesive and self-healable hydrogel-based wearable strain sensor for human motion and physiological signal monitoring, J. Mater. Chem. B 7 (30) (2019) 4638–4648, https://doi.org/10.1039/C9TB01039D.

[36] C. Ma, Y.i. Wang, Z. Jiang, Z. Cao, H. Yu, G. Huang, Q.i. Wu, F. Ling, Z. Zhuang, H. Wang, J. Zheng, J. Wu, Wide-range linear viscoelastic hydrogels with high mechanical properties and their applications in quantifiable stress-strain sensors, Chem. Eng. J. 399 (2020) 125697, https://doi.org/10.1016/j.cej.2020.125697.

[37] L. Shi, P. Ding, Y. Wang, Y.u. Zhang, D. Ossipov, J. Hilborn, Self-healing polymeric hydrogel formed by metal–ligand coordination assembly: design, fabrication, and biomedical applications, Macromol. Rapid Commun. 40 (7) (2019) 1800837, https://doi.org/10.1002/marc.201800837.

[38] K. Zhang, Q. Feng, J. Xu, X. Xu, F. Tian, K.W.K. Yeung, L. Bian, Self-assembled injectable nanocomposite hydrogels stabilized by bisphosphonate-magnesium (Mg2+) coordination regulates the differentiation of encapsulated stem cells via dual crosslinking, Adv. Funct. Mater. 27 (2017) 1–11, https://doi.org/10.1002/adfm.201701642.

[39] L. Shi, F. Wang, W. Zhu, Z. Xu, S. Fuchs, J. Hilborn, L. Zhu, Q.i. Ma, Y. Wang, X. Weng, D.A. Ossipov, Self-healing silk fibroin-based hydrogel for bone regeneration: dynamic metal-ligand self-assembly approach, Adv. Funct. Mater. 27 (37) (2017) 1700591, https://doi.org/10.1002/adfm.201700591.

[40] K. Zhang, Z. Jia, B. Yang, Q. Feng, X. Xu, W. Yuan, X. Li, X. Chen, L.i. Duan, D. Wang, L. Bian, Adaptable hydrogels mediate cofactor-assisted activation of biomarker-responsive drug delivery via positive feedback for enhanced tissue regeneration, Adv. Sci. 5 (12) (2018) 1800875, https://doi.org/10.1002/advs.201800875.

[41] R.K. Das, V. Gocheva, R. Hammink, O.F. Zouani, A.E. Rowan, Stress-stiffening-mediated stem-cell commitment switch in soft responsive hydrogels, Nature Mater 15 (3) (2016) 318–325, https://doi.org/10.1038/nmat4483.

[42] R.S. Rivlin, A.G. Thomas, Rupture of rubber. I. Characteristic energy for tearing, J. Polym. Sci. 10 (1953) 291–318, https://doi.org/10.1002/pol.1953.120100303.

[43] W. Feng, W. Zhou, S. Zhang, Y. Fan, A. Yasin, H. Yang, UV-controlled shape memory hydrogels triggered by photoacid generator, RSC Adv. 5 (100) (2015) 81784–81789, https://doi.org/10.1039/C5RA14421C.

[44] S. Çavuş, Poly(methacrylamide- co -2-acrylamido-2-methyl-1-propanesulfonic acid) hydrogels: Investigation of pH- and temperature-dependent swelling characteristics and their characterization, J. Polym. Sci. Part B Polym. Phys. 48 (2010) 2497–2508, https://doi.org/10.1002/polb.22152.

[45] F.A. Cotton, G. Wilkinson, Advanced Inorganic Chemistry, Fourth, John Wiley & Sons, Inc., 1963 https://doi.org/10.1021/ic50007a079.

[46] J.L. Lippert, J.A. Robertson, J.R. Havens, J.S. Tan, Structural studies of poly(N-vinylimidazole) complexes by infrared and Raman spectroscopy, Macromolecules 18 (1) (1985) 63–67, https://doi.org/10.1021/ma00143a010.

[47] T. Nonoyama, Y.W. Lee, K. Ota, K. Fujioka, W. Hong, J.P. Gong, Instant thermal switching from soft hydrogel to rigid plastics inspired by thermophile proteins, Adv. Mater. 32 (4) (2020) 1905878, https://doi.org/10.1002/adma.201905878.

[48] T.L. Sun, T. Kurokawa, S. Kuroda, A.B. Ihsan, T. Akasaki, K. Sato, M.A. Haque, T. Nakajima, J.P. Gong, Physical hydrogels composed of polyampholytes demonstrate high toughness and viscoelasticity, Nat. Mater 12 (10) (2013) 932–937, https://doi.org/10.1038/nmat3713.

[49] P. Panda, A. Dutta, D. Ganguly, S. Chattopadhyay, R.K. Das, Engineering hydrophobically associated hydrogels with rapid self-recovery and tunable mechanical properties using metal-ligand interactions, J. Appl. Polym. Sci. 137 (48) (2020) 49590, https://doi.org/10.1002/app.49590.

[50] D.E. Fullenkamp, L. He, D.G. Barrett, W.R. Burghardt, P.B. Messersmith, Mussel-inspired histidine-based transient network metal coordination hydrogels, Macromolecules 46 (3) (2013) 1167–1174, https://doi.org/10.1021/ma301791n.

[51] V.T. Tran, M.T.I. Mredha, S.K. Pathak, H. Yoon, J. Cui, I. Jeon, Conductive tough hydrogels with a staggered ion-coordinating structure for high self-recovery rate, ACS Appl. Mater. Interfaces 11 (27) (2019) 24598–24608, https://doi.org/10.1021/acsami.9b06478.s006.

[52] W.C. Yount, D.M. Loveless, S.L. Craig, Small-molecule dynamics and mechanisms underlying the macroscopic mechanical properties of coordinatively cross-linked

polymer networks, J. Am. Chem. Soc. 127 (41) (2005) 14488–14496, https://doi.org/10.1021/ja054298a.s001.
[53] W.C. Yount, D.M. Loveless, S.L. Craig, Strong means slow: dynamic contributions to the bulk mechanical properties of supramolecular networks, Angew. Chem. Int. Ed. 44 (18) (2005) 2746–2748, https://doi.org/10.1002/anie.200500026.
[54] O. Chaudhuri, L. Gu, M. Darnell, D. Klumpers, S.A. Bencherif, J.C. Weaver, N. Huebsch, D.J. Mooney, Substrate stress relaxation regulates cell spreading, Nat Commun 6 (1) (2015), https://doi.org/10.1038/ncomms7365.
[55] N.S. Schauser, G.E. Sanoja, J.M. Bartels, S.K. Jain, J.G. Hu, S. Han, L.M. Walker, M. E. Helgeson, R. Seshadri, R.A. Segalman, Decoupling bulk mechanics and mono- and multivalent ion transport in polymers based on metal–ligand coordination, Chem. Mater. 30 (16) (2018) 5759–5769, https://doi.org/10.1021/acs.chemmater.8b02633.s001.
[56] X. Xiao, W. Liu, K. Wang, C. Li, X. Sun, X. Zhang, W. Liu, Y. Ma, High-performance solid-state Zn batteries based on a free-standing organic cathode and metal Zn anode with an ordered nano-architecture, Nanoscale Adv. 2 (1) (2020) 296–303, https://doi.org/10.1039/C9NA00562E.
[57] I. Hussain, S.M. Sayed, S. Liu, O. Oderinde, M. Kang, F. Yao, G. Fu, Enhancing the mechanical properties and self-healing efficiency of hydroxyethyl cellulose-based conductive hydrogels via supramolecular interactions, Eur. Polym. J. 105 (2018) 85–94, https://doi.org/10.1016/j.eurpolymj.2018.05.025.
[58] T. Long, Y. Li, X.u. Fang, J. Sun, Salt-mediated polyampholyte hydrogels with high mechanical strength, excellent self-healing property, and satisfactory electrical conductivity, Adv. Funct. Mater. 28 (44) (2018) 1804416, https://doi.org/10.1002/adfm.201804416.
[59] C. Yang, Z. Suo, Hydrogel ionotronics, Nat. Rev. Mater. 3 (6) (2018) 125–142, https://doi.org/10.1038/s41578-018-0018-7.
[60] J.-Y. Sun, C. Keplinger, G.M. Whitesides, Z. Suo, Ionic skin, Adv. Mater. 26 (45) (2014) 7608–7614, https://doi.org/10.1002/adma.201403441.
[61] G. Cai, J. Wang, K. Qian, J. Chen, S. Li, P.S. Lee, Extremely stretchable strain sensors based on conductive self-healing dynamic cross-links hydrogels for human-motion detection, Adv. Sci. 4 (2) (2017) 1600190, https://doi.org/10.1002/advs.201600190.
[62] T. Yamada, Y. Hayamizu, Y. Yamamoto, Y. Yomogida, A. Izadi-Najafabadi, D. N. Futaba, K. Hata, A stretchable carbon nanotube strain sensor for human-motion detection, Nat. Nanotech. 6 (5) (2011) 296–301, https://doi.org/10.1038/nnano.2011.36.
[63] S. Liu, L. Li, Ultrastretchable and self-healing double-network hydrogel for 3D printing and strain sensor, ACS Appl. Mater. Interfaces 9 (31) (2017) 26429–26437, https://doi.org/10.1021/acsami.7b07445.s001.
[64] C.G. Dobie, W.B. Isaac Peter, Electric Resistance Strain Gauges, English Universities Press Limited, 1948.
[65] B. Xu, P. Zheng, F. Gao, W. Wang, H. Zhang, X. Zhang, X. Feng, W. Liu, A Mineralized High Strength and Tough Hydrogel for Skull Bone Regeneration, Adv. Funct. Mater. 27 (4) (2017) 1604327, https://doi.org/10.1002/adfm.201604327.
[66] Y. Liu, J. Liu, H. Yang, K. Liu, R. Miao, H. Peng, Y. Fang, Dynamic covalent bond-based hydrogels with superior compressive strength, exceptional slice-resistance and self-healing properties, Soft Matter 14 (39) (2018) 7950–7953, https://doi.org/10.1039/C8SM01742E.
[67] M.T.I. Mredha, H.H. Le, V.T. Tran, P. Trtik, J. Cui, I. Jeon, Anisotropic tough multilayer hydrogels with programmable orientation, Mater. Horiz. 6 (7) (2019) 1504–1511, https://doi.org/10.1039/C9MH00320G.